Accurate and Efficient Multi-scale Flow Simulation using a Hybrid CFD-MD Approach ***Jeff: Another recommendation: Numerical and Computational Investigations on Hybrid CFD-MD Simulations

Soon-Heum Ko[a], Nayong Kim[a], Dimitris Nikitopoulos[c], Dorel Moldovan[c], Shantenu Jha[a,b,*]

[a]Center for Computation & Technology, Louisiana State University, Baton Rouge, LA 70803, USA
[b]Department of Computer Science, Louisiana State University, Baton Rouge, LA 70803, USA
[c]Department of Mechanical Engineering, Louisiana State University, Baton Rouge, LA 70803, USA

Abstract

We investigate numerical and computational issues on a hybrid computational fluid dynamics (CFD) - molecular dynamics (MD) simulation in this paper. Current hybrid simulation framework is based on reliable CFD and MD codes and it is incorporated with hybrid interfaces along with the coupling scheme of constrained Lagrangian dynamics. We argue that (1) statistical error of sampled molecular solution and (2) hybrid boundary conditions via the extrapolation have been causing spatial and temporal inaccuracies in hybrid simulations. We propose determining coupling parameters through the statistical noise analysis of a stationary flow and sampling multiple independent replicas as two solutions for minimizing the influence of this spatial/temporal locality. Also, we design a new temporal coupling scheme called 'a prediction-correction approach' which provides a time-accurate hybrid boundary condition through interpolation. With respect to computational performance, concurrent starting of logically distributed components

*Corresponding author, (Tel)+1-225-578-XXXX; (FAX)+1-225-578-XXXX

Email addresses: sko@cct.lsu.edu (Soon-Heum Ko), nykim@cct.lsu.edu (Nayong Kim), meniki@me.lsu.edu (Dimitris Nikitopoulos), moldovan@me.lsu.edu (Dorel Moldovan), sjha@cct.lsu.edu (Shantenu Jha)

and load balancing among these tasks are two important considerations in all coupled simulations. We exploit a BigJob framework, which is a kind of Pilot-Job, and incorporate the load balancing function to overcome above computational difficulties of coupled simulations. Developed hybrid framework is utilized in solving nano-scale fluid systems. The accurate modeling of sampling noise is accomplished by the stationary flow simulation and multiple sampling approach is applied to explore the accuracy of hybrid simulation technique in relatively low-speed flow fields of O(10) m/s velocity. Also, the accuracy of a new temporal coupling scheme is evaluated by solving the oscillating boundary problem. Finally, computational costs with or without a BigJob framework are investigated to evaluate the performance of the current hybrid simulation framework.

1. Introduction and Motivation

A hybrid continuum dynamics - particle dynamics approach is defined as expressing macroscopic flow physics by the continuum hypothesis while capturing the complex flow characteristics around obstacles by solving finer-resolution particle dynamics. The hybrid method is more accurate than the traditional Computational Fluid Dynamics (CFD) technique, since it does not require empirical boundary condition modeling in describing intermolecular effect near the solid-fluid interface. Also, the hybrid approach provides a better computational efficiency than particle dynamics simulation by replacing numerous particles in moderate flow regime to sparser continuum mesh system. In this section, we address a number of previous studies on the hybrid simulation and raise unsolved numerical and computational difficulties which shall be covered in this paper.

1.1. Previous Works ****Jeff: Who can change the title more elegantly?*

Hybrid simulation approaches can be grouped into two according to the microscopic solution method coupled into macroscopic continuum domain. [1] One is the coarse-grained particle simulations by using Direct Simulation Monte Carlo (DSMC) for dilute gas [2, 3] or Dissipative Particle Dynamics (DPD) for liquid [4, 5], where the simulation molecule represents a number

of atoms/molecules. The coarse-grained simulation can provide better computational cost, while the state-of-the-art modeling is required to correctly impose the wall boundary condition. The other is the use of traditional Molecular Dynamics (MD) solvers that describe the motion of individual molecules based on Newtonian dynamics. The hybrid CFD-MD model is preferred in solving dense liquid systems where the accurate description of strong inter-molecular interaction near the solid obstacle is very important.

Hybrid CFD-MD simulations can be classified to constrained Lagrangian dynamics [6–12], alternating Schwarz method [13–17], and direct flux exchange [18–23], according to which variables are exchanging and how the macroscopic solution is imposed on molecular domain. O'Connell and Thompson [6] first tried a hybrid CFD-MD simulation by applying constrained Lagrangian dynamics in the overlapping region between CFD and MD domains. In this method, two solvers exchange density properties (in other words, conserved variables) in the overlapping boundary and they are coupled in time space. Constrained Lagrangian dynamics equation is used to accelerate/decelerate particles in hybrid MD boundary to follow the continuum velocity, without harming the degree-of-freedom of molecular motion. This approach is refined by Nie *et al.* [7] by including the mass flux modeling and has been applied to the sudden-start Couette flow [6], channel flow with rough walls [7], cavity flow [8], Poiseuille flow [11] and the oscillating boundary problem [10, 12]. The use of a straightforward constrained dynamics equation makes this approach easy to implement and computationally efficient. However, the absence of energy exchange modeling limits the applications to isothermal systems. [18]

Hadjiconstantinou and his collaborators [13–15] proposed another hybrid simulation approach which is based on alternating Schwarz method. In this approach, continuum solution is imposed on particle domain by using Maxwellian distribution function [14] or Chapman-Enskog distribution function [2]. CFD and MD solvers are evolving in individual time space until solutions in the overlapping region become identical. This approach is further expanded to non-periodic boundary condition problems by Werder *et al.* [16], who also refined previous boundary force models [6, 7, 18, 20] by minimizing the local disturbance. Alternating Schwarz approach has been applied to moving contact line problem [14], Poiseuille flow [15], flow around the cylinder [16], and Couette flow of water [17]. The characteristics of decoupled time space between two domains makes this approach better in solving the flow field where hydrodynamic characteristic timescale is much larger

3

than molecular dynamic timescale, i.e., micrometer system size. [14] However, the feature of decoupling in time space limits this approach to steady or quasi-steady flow simulations. [18]

The direct flux exchange approach exchanges flux properties along the interface of CFD and MD domains at the same physical time. Flekkϕy et al. [18] first proposed a model for solving an isothermal flow and the model is improved by considering energy transfer [19, 20]. Also, Delgado-Buscalioni and Coveney [21] designed a particle insertion algorithm which satisfies the mass flux along the interface while preserving the mean potential energy of a system. This approach has been applied to solving Couette and Poiseulle flow [18], transversal wave [20], and oscillating boundary problem [22]. According to Flekkϕy et al. [18], flux exchange directly implies adherence to the relevant conservation laws without the use of constitutive relations and equations of state (to maintain the conservation laws). However, it is pointed out that the sampling time to measure fluxes within acceptable statistical error is orders of magnitude larger than the time to measure densities [15].

***Jeff: Summary: Alternating Schwarz: decoupled in time domain / exchange density Good for large system simulation (10-6 or bigger) / steady or quasi-steady solutions Direct flux: coupled in time domain / exchange flux Good for highly varying unsteady flow field in nanoscale with strong secondary flow / sampling time can be large compared to characteristic time in nano-scale systems Constrained Lagrangian dynamics: coupled in time domain / exchange density Good for unsteady moderate flow where secondary flow normal to principal direction is not strong + efficient / isothermal Comparing these models by their initial formulation, alternating Schwarz model decouples time domain between continuum and atomistic solvers while other two models couple the time domain. Regarding the coupled properties, direct flux scheme exchanges fluxes between two domains while other two methods match conserved properties. Thus, alternating Schwarz method requires less cost for solving a steady flow over a long time range and direct flux exchange is adequate for solving complex nano-scale flowfield. Constrained Lagrangian dynamics has good performance. As time evolves, each technique has improved to accept others' benefit, thus it becomes meaningless to discuss on one's superiority over other models at this point.

1.2. Numerical and Computational Issues

Despite the clear advantage of hybrid approach over conventional CFD or MD implementations, a number of numerical and computational difficul-

ties prohibit this technique from being widely used. The first issue is an easy and intuitive way of determining the state-of-the-art coupling condition. The solution of a hybrid simulation by the crude coupling suffers from a strong noise of spatially averaged particle velocity, which is the response of a natural physics of molecular fluctuation. So, coupling parameters such as layer size and the position of overlap region, and sampling duration with its interval, should be delicately determined to achieve an accurate numerical solution. It is impossible to design a mathematical model to determine coupling conditions, since the strength of this uninvited noise is affected by not only the flow condition but also the characteristics of fluid and solid elements along with its geometric configuration. There have been some attempts to alleviate this statistic fluctuation by introducing numerical damping terms [6, 9] or dynamic parameter for coupling intensity [10], but this can break up the conservation law.

The next issue is the hybrid simulation in moderate flow conditions. So far, all experiments have been confined to the extremely high-speed flow conditions of O(100) m/s in the nano-scale systems, to maintain a strong shear rate/speed in the overlapping region. This unrealistic flow condition is unavoidable according to the mathematical analyses on the strength of statistical error (in other words, a signal-to-noise ratio) [15, 22]. Sampling duration to maintain the same statistical error is proportional to $1/u_\infty{}^2$ and $1/N_0$, where u_∞ is a free stream condition and N_0 denotes the number of particles contained in sampling layer. So, reducing the free stream velocity by 1/10 requires 100 times more particles to be averaged to maintain the same statistical error. (Increasing the sampling duration is avoided because it can fail to describe the unsteady flow evolution.) This necessitates a different design of a hybrid simulation framework.

The accuracy of temporal coupling scheme with boundary condition imposition is of another importance in solving the unsteady problems. Temporal coupling scheme denotes the scheduling of data exchange routine in time space between CFD and MD solvers, to synchronize both solutions at the same physical time. As to be discussed in Section 2.5 in detail, initial models inherently contain the time-lagging phenomenon because backward-averaged molecular dynamic properties is adopted as the instantaneous solution at continuum domain. As the remedy, Liu *et al.* [12] proposed a multi-timescale algorithm by considering quasi-steadiness and Wang and He [10] proposed passing the extrapolated continuum solution to the MD solver. However, a multi-timescale algorithm is only valid if the period of unsteady phenomenon

is sufficiently longer than sampling duration and particles lose their history during the re-initialization process in between sampling interval: Approach by Wang and He is a possible approach to mitigate the time-lagging effect though not in perfection.

In addition to above numerical issues, there also exist computational challenges of integrating multiple application domains into a single problem set. Considering very different computational kernels (one could be mesh-based, the other unstructured particle simulations), it is nearly impossible to incorporate distinct CFD and MD codes under the umbrella of a single tightly-coupled application (i.e., unifying two application codes to share a single MPI communicator). One possible alternative will be to implement coupling interface on individual code and control these logically separated codes as a virtually unified simulation package.

However, confined to parallel execution on conventional production system with batch queue, it cannot be guaranteed that two separate jobs will execute concurrently. Considering the computational characteristics of current application, where CFD and MD codes conduct frequent information exchange, the first job to run will inevitably experience the idle waiting for its counterpart without the explicit support for co-scheduling. Another important challenge is the need for efficient load-balancing which takes into account the individual application's performance. Even if the two simulations could run concurrently, without explicit load-management/balancing support, there is likely to be inefficient utilization of compute resources due to load imbalance. As the performance of each simulation component changes with computing resource and problem size, re-adjustment of allocated resources to each task according to their performance is required during the simulation.

1.3. Objectives and Outline of the Paper

We are focusing on investigating numerical issues of applying the hybrid CFD-MD scheme to a nano-fluidic system, as well as designing and developing an efficient runtime framework for a coupled multi-component simulation. We consider the implementation of a 'generic' hybrid interface which can be easily attached to various kinds of incompressible CFD codes and MD packages, and the building of a 'portable' framework which is acceptable for most computer architectures.

Regarding numerical simulation, we develop the hybrid simulation framework based on the constrained Lagrangian dynamics and apply it to pro-

totype examples. We propose the determination of coupling parameters based on the strength of statistical noise in stationary flow. Also we explore to the moderate-speed flow simulation in O(10) m/s velocity, which is the first successful analysis by a hybrid approach. Excessive statistical noise in this flow condition is shrunk by sampling multiple individual experiments. For physically unsteady flow simulation, we design a novel temporal coupling scheme, named 'prediction-correction approach'. Compared to conventional scheme, our approach provides better accuracy by eliminating the overshoot/undershoot phenomena and diminishing the time-lagging pattern.

In view of computational science, we believe our trial is the first documented coupled multi-physics simulation utilizing a virtually unified simulation package, called "Pilot-Job". We claim that there are several distinct advantages of using Pilot-Job: (i) obviates the need for a co-scheduler while preserving performance, (ii) enables dynamic resource allocation, which in turn is important for load-balancing across coupled simulations.

We begin the next section with the numerical details of individual CFD and MD code and implementation of hybrid interface. The construction of an efficient CFD-MD simulation framework will be discussed in Section 3. In Section 4, we will demonstrate our numerical results of a famous validation problem (a sudden-start Couette flow) and the physically unsteady flow simulation (oscillating boundary problem). The performance of this coupled simulation is described in Section 5. Finally, our next plan and the summary of current work are expressed in Sections 6 and 7.

2. Fundamentals of Hybrid Coupled Continuum-Molecular Simulation Toolkit

The accuracy of a hybrid CFD-MD solution is governed by the underlying numerical schemes in individual solver as well as hybrid schemes implemented. We explain the features of baseline solvers and the structure of hybrid interface in this section. We also investigate additional numerical treatments to improve the accuracy of hybrid CFD-MD simulations in various types of fluid systems.

2.1. Overview of the Continuum-Molecular Coupled Approach

The hybrid CFD-MD approach stands on the proposition that the molecular dynamic simulation produces more accurate solution than the continuum model and a more efficient continuum solver provides the boundary condition

7

to particle domain without restricting the high degree-of-freedom of atom-istic motion. So, the region which contains a strong flow gradient is resolved by a molecular dynamic simulation and moderate flow in macroscopic scale is captured by the continuum dynamics. Also, these problem domains overlap each other in the middle to exchange the individual information.

A detailed structure of the fluid domain for constrained Lagrangian dy-namics models is described in Fig. 1. CFD approach solves the external zones with the moderate flow velocity and MD analyzes the complex microscopic flow feature near the stationary obstacle or in the low-speed region. Hybrid region is placed sufficiently far from the solid obstacle to prevent the direct influence of strong fluctuation near the solid-fluid interface. Also, this region is designed sufficiently large to contain five layers with enough spacing.

Roles of these layers in hybrid region are as follows. From the bottom, we have the *particle-to-continuum* and *continuum-to-particle* (denoted as 'MD-toCFD' and 'CFDtoMD', respectively) boundary zones for CFD and MD simulations, and have additional zone to exert external force. These three interesting zones are isolated by the buffer in between. Particles' proper-ties spatially located in the MDtoCFD boundary layer are averaged over a finite time (called 'sampling duration') and they are transferred to contin-uum solver at constant period (called 'sampling interval'). The height of each layer is the same as the CFD cell height and averaged conservative properties in two consecutive layers are passed to continuum domain to be directly imposed as the viscous boundary condition on the Navier-Stokes solver with collocated data structure. Next, the hybrid MD boundary zone is placed in the middle. In this region, the instantaneous continuum solution is transferred to MD code. Particles in this layer are guided to eventually follow this macroscopic flow velocity, by solving a constrained Lagrangian dynamics equation. The strong point of this equation is that, molecules are led to follow the macroscopic flow property, while preserving their degree-of-freedom of translational motion. In the uppermost layer, the external force is exerted on particles to conserve system's statistical ensembles. This force function is designed not too strong to influence the motion of particles in the domain of interest nor not too weak to have particles drifting away. Finally, buffer layer is positioned in between each layer. This layer is set up to be bigger than the length scale of interacting particles (cutoff radius), not to have a solution in one layer being directly interfered by another solution.

***Jeff: It would be better to explain a little more detail on last sen-tence. Let's say the buffer between CFDtoMD and MDtoCFD boundary is
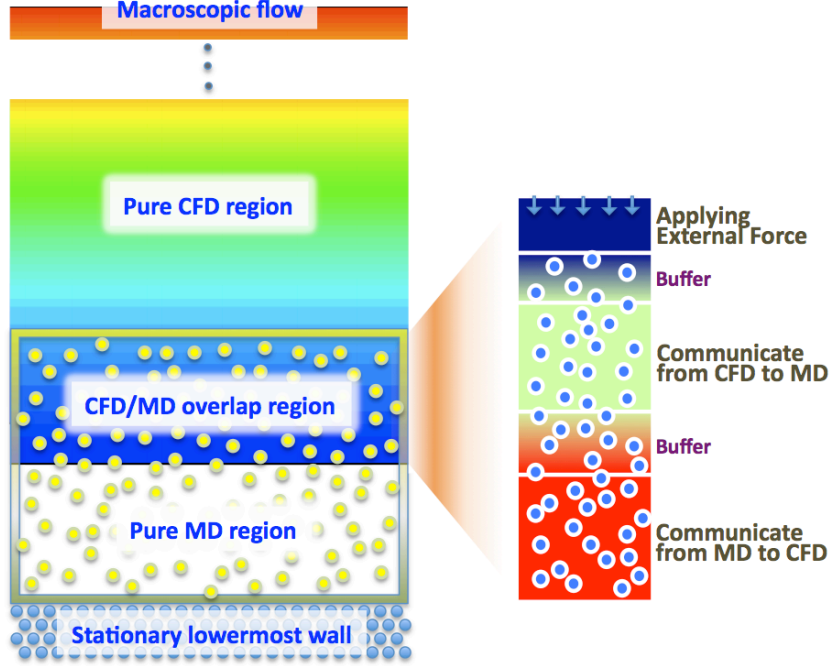
Figure 1: Schematic Diagram of the Hybrid Domain with Detailed View of Overlapping Zone; Overall continuum/atomistic computational domain including overlap region is shown on left figure. Detailed layer by layer explanation of overlapping region is indicated by right figure.

smaller than cutoff length. Then, a solution at CFDtoMD (constrained MD) directly affects the motion of particles at MDtoCFD. And this is used for CFD boundary condition. This results that, CFD solution at CFDtoMD is the result of flow variation in MDtoCFD boundary, which in turn is directly affected by the CFDtoMD solution. Thus, solution at CFDtoMD becomes the boundary condition of CFD domain.

2.2. Governing Equations and Numerical Schemes

2.2.1. Continuum Incompressible Flow Formulation (CFD)

The current in-house continuum hydrodynamics code solves the unsteady incompressible Navier-Stokes equations to demonstrate the isothermal nanoscale flow field:

$$\frac{\partial u_i}{\partial x_i} = 0 \tag{1}$$

9

$$\frac{\partial u_i}{\partial t} + \frac{\partial}{\partial x_j}(u_i u_j) = -\frac{\partial p}{\partial x_i} + \nu \frac{\partial^2 u_i}{\partial x_j \partial x_j}$$

where ν is the kinematic viscosity.

In this work, we adopted the pseudo-compressibility method [24] to form a hyperbolic system of equations which can be marched in pseudo-time. A time derivative of pressure is added to the continuity equation resulting in

$$\frac{\partial(p/\rho)}{\partial \tau} = -\beta \frac{\partial u_i}{\partial x_i} \tag{2}$$

where β denotes a pseudo-compressibility parameter, currently set up as 2.5.

For time-accurate unsteady simulation, dual time stepping method is adopted and it is combined with the LU-SGS (Lower-Upper Symmetric Gauss-Seidel) scheme [25] for the implicit time integration. The inviscid fluxes are upwind-differenced using Osher's flux-difference splitting scheme [26]. For higher-order spatial accuracy, the MUSCL (Monotone Upstream-centered Schemes for Conservation Laws) [27] approach is used on inviscid flux calculation. Viscous fluxes are calculated using the conventional second-order central differencing.

2.2.2. Molecular-Level Formulation (MD)

In MD, an initial velocity is assigned to each atom, and Newton's laws are employed at the atomic level to propagate the system's motion through time evolution. To calculate pairwise interactions of particles in the system, the most commonly used Lennard-Jones (12-6) potential interaction model is employed and is define as:

$$u(|r_i - r_j|) = 4\epsilon_{ij}[(\frac{\sigma_{ij}}{r_{ij}})^{12} - (\frac{\sigma_{ij}}{r_{ij}})^6] \tag{3}$$

where ϵ_{ij} and σ_{ij} denote the pairwise potential well depth and the atom size parameter respectively, and r_{ij} is the distance between the particle i and j. The term $1/r_{ij}^{12}$ dominating at short range distance repulsive behavior based on the Pauli principle to avoid overlapping the electronic clouds when particles are brought very close to each other. The term $1/r_{ij}^6$ dominates at long range attractive forces by van der Waals dispersion forces. The cut-off

10

Table 1: Implementation of Hybrid Interface on CFD and MD Codes. Both codes are equipped with the file-based information exchange routine, to update the hybrid boundary condition. CFD code experiences the global change of its data structure to store the information of the entire fluid system. MD code adopts hybrid equations to impose the macroscopic information on microscopic domain and to ensure numerical stability.

	CFD	MD
Global Change	Overset Data Structure (*optional*)	-
External Force	-	External Force Equation (Eqn. 4)
CFDtoMD	File Interface: Sender	File Interface: Receiver Constrained MD Equation (Eqn. 10)
MDtoCFD	File Interface: Receiver	File Interface: Sender

distance σ_c is introduced here to reduce the computational cost and is set to be 2.2σ [28].

The time integration algorithm is required to integrate the equation of motion of the interacting particles and computing molecular trajectories, one of most common velocity Verlet algorithm is employed to compute the simulation.

In this work, the MD simulations were performed by using the modified version of Large Atomic Molecular Massively Parallel Simulator(LAMMPS). It is the classical molecular dynamics open-source code written in C++ and developed by Sandia National Labs. [29]

2.3. Hybrid Interfaces and Schemes

The hybrid simulation requires the implementation of hybrid interfaces and schemes on individual code. In the current study, the file interface is designed to schedule the information exchange between continuum and discrete particle descriptions. A constrained Lagrangian dynamics model is implemented for hybrid simulation. Unit conversion routine is also implemented in the application code. These changes are summarized in table 1.

The CFD code employs the data structure of overset mesh technique [30] to ease the handling of coupling parameters. In other words, the entire fluid domain is generated as the CFD mesh system and pure MD region is turned off as the 'Hole' cell in the terminology of overset technique. Likewise, MD-

toCFD and CFDtoMD boundary cells are declared as 'Fringe' and 'Donor' cells, respectively. The labor of mesh regeneration according to the change of coupling parameters (position and depth of hybrid layers) disappears with the overset data structure.

Both codes are equipped with the information exchange routine which consists of one file sender and one file receiver. These file interfaces are scheduled to turn on every sampling interval. The instantaneous properties in the Donor cells of continuum domain are transferred to MD site and referenced when applying constrained Lagrangian dynamics equation. Averaged molecular properties are sent to CFD domain and they are used as the boundary conditions of Fringe cells. All exchanged properties are written in MD unit: thus, CFD code is equipped with velocity unit conversion function and equation of state which changes the pressure solution from CFD site to equivalent density property in MD domain.

Along with the file interface, additional equations of motion are employed on MD code to accurately describe the influence of macroscopic flow variation on particle domain. First, the external force should be imposed to prevent leaving particles from the control domain and the force is applied to the normal direction of uppermost MD layer. A cost-effective classical external force model by Nie et $al.$ [7] is employed as,

$$F_{ext,i} = -p_a \sigma \frac{y_i - Y_{n-1}}{1 - (y_i - Y_{n-1})/(Y_n - Y_{n-1})} \tag{4}$$

where p_a denote the average pressure in the MD region, $Y_n - Y_{n-1}$ is the thickness of the uppermost layer which is applied the force and F_{ext} is the external force acting on i^{th} particle located on position y_i.

Next, on CFDtoMD layer, the macroscopic flow properties at specific time shall be introduced to lead the motion of multiple particles in that layer. To satisfy mass conservation, a certain number of particles are inserted into or removed from this layer according to the mass flux by CFD solution,

$$n = -A\rho u_y \Delta t / m \tag{5}$$

where A is the horizontal area, u_y is the vertical velocity component by CFD solution and Δt is the sampling interval.

A very complicated numerical intervention is required to maintain momentum conservation. The average velocities of particles in J_{th} cell is equal to the velocity u_J in continuum cell.

$$u_J(t) = \frac{1}{N_J} \sum_i v_i \tag{6}$$

where v_i is velocity of ith particle and N_J is the number of particles in the cell. With taking Lagrangian derivative of Eq. 6,

$$\frac{Du_J(t)}{Dt} = \sum_i \frac{\ddot{x}_i}{N_J} \tag{7}$$

The Classical MD equation of motion can be generalized to obtain constraint by adopting the fluctuation in acceleration of each particles, ζ_i

$$\frac{F_i}{m_i} = \ddot{x}_i(t) = \frac{Du_J(t)}{Dt} + \zeta_i = \frac{\sum\limits_i F_i(t)}{\sum\limits_i m_i} + \zeta_i \tag{8}$$

where F_i is the force on i^{th} particle based on the interactions between particles, m_i is mass of each atom and Eqn. 9 satisfies,

$$\sum_i \zeta_i m_i = 0 \tag{9}$$

Finally, the constrained particle dynamics with conventional equation of motion can be written as:

$$\ddot{x}_i(t) = \frac{F_i}{m_i} - \frac{\sum\limits_i F_i(t)}{\sum\limits_i m_i} - \frac{1}{\Delta t_{MD}} \{ \frac{\sum\limits_i m_i \dot{x}_i}{\sum\limits_i m_i} - u_J(t + \Delta t_{MD}) \} \tag{10}$$

The continuum velocity and the mean microscopic velocity from MD over control domain provide the synchronization of the mass and momentum consistent with Eqn. 10.

2.4. Statistical Error and Coupling Parameters

How to reduce the statistical error of averaged MD profile, which is the response of innate spatial/temporal locality in molecular dynamic systems, determines the accuracy of CFD solution in hybrid simulation. According

to the mathematical expression in statistical error [15, 22], the ratio of sampling noise compared to the macroscopic velocity is inversely proportional to the square root of spatial layer size and temporal sampling duration. For example, reducing the macroscopic velocity by half requires either 4 times larger system domain or 4 times longer sampling to maintain the same order of accuracy.

Sampling duration with interval, the size of sampling layer and its position are coupling parameters which define the scale and pattern of this noise. The layer size and sampling duration collectively work for reducing the noise, by increasing the spatial and temporal sampling scales. Sampling interval is a factor which restricts the sampling duration. On unsteady simulations, a short sampling interval is preferred to frequently update temporal variation of flow field in hybrid boundary zones. This interval acts as the upper bound of sampling duration. The location of the sampling layer is a secondary factor which can locally increase the strength of fluctuation. Conventionally, sampling layer is placed far from the solid obstacle, e.g., at least 10 σ above the bottom wall in solving the flow of the liquid argon [11].

We introduce two numerical ideas to acquire the accurate hybrid solution. One is to quantitatively measure the scale of statistical noise in particular domain and the other is to numerically get the acceptable solution. The former shows the initial guideline to determine the coupling parameter and the latter refines the accuracy of the former solution.

2.4.1. Determining Coupling Conditions

The statistical noise is a function of the characteristics of fluid and surrounding solid elements, and geometric configurations, as well as the flow condition. Unfortunately, previous analyses on the strength of statistical error [15, 22] fails to consider the stronger interaction near the fluid-solid interface and the shape of the domain. We sense that the clear coupling parameters can be determined after the look-up of that specific system

Our intuitive idea of numerically detecting the strength of statistical noise is to solve the stationary flow of the same fluid domain by pure MD method. The procedure is as follows.

1. Empirical design of the sampling interval and the sampling layer's position[1]
2. Structure construction[2]
3. Simulation and collecting the temporal history of sampled velocity[3]

14

4. Data processing[4]

5. Determining the sampling layer size and the sampling duration[5,6]

We argue that our idea is very easy to follow and computationally not expensive since the solution of the stationary flow is immediately collected. This stationary flow simulation provides the amount of sampling noise in various sampling conditions. Meanwhile, this experiment does not provide the statistical error because of the impossibility to predict the macroscopic velocity expect some well-known flow systems. This necessitates us to investigate additional approach which is globally applicable.

2.4.2. Sampling Multiple Independent Experiments

So far, all hybrid CFD-MD applications have been restricted to extremely fast flow field of O(100) m/s velocity. The difficulty of solving moderate-speed flow field by a hybrid approach is explained as follows. The hydrodynamic time scale is expressed as a function of characteristic size and kinematic viscosity. This implies that the sampling interval is fixed regardless of the change in velocity. This, in turn, results in the impossibility to handle the sampling duration. Increasing the system size proportional to the square of the velocity change remains the only possible way to maintain the same statistical accuracy. Unfortunately, submitting excessively large-scaled simulation on

---

[1]Sampling interval is designed less than $1/100^{th}$ of hydrodynamic characteristic time; The location of sampling layer is placed O(10) nanometers above the solid obstacle.

[2]The height of the domain can be reduced by placing a specular wall on the top, in case the system is sufficiently large; The length of the domain along the periodic direction can be arbitrarily chosen. The optimal length is further determined by the relation between the strength of noise and number of particles, i.e., $V_{noise} \propto 1/\sqrt{N}$.

[3]Data collection starts as soon as the relaxation process is finished. Temporal history of averaged velocity from the smallest layer size with shortest sampling interval is stored.

[4]Produced dataset around the location of sampling layer is spatially and temporally averaged to produce the spatial and temporal variation of the sampled velocity.

[5]The noise is compared with the expected macroscopic velocity at that position, considering the linear velocity gradient from the wall to the far field. A paired condition which produces sufficiently small portion of noise and whose temporal duration is less than designed sampling interval is chosen to be the layer size and sampling duration of this hybrid simulation.

[6]If no condition is satisfactory, the acceptable condition can be obtained by either increasing the length of computational domain based on $V_{noise} \propto 1/\sqrt{N}$ or changing the position of sampling layer and repeating data processing. The one condition which generates the smallest MD domain in the hybrid simulation is chosen.

public supercomputers unfavorably takes far long time to get allocated. In worse case, the simulation may exceed the capacity of the system. Thus, a different approach is necessary for efficiently simulating the low-speed flow field.

We propose sampling multiple independent hybrid simulations from a smaller domain instead of trying to run a single hybrid simulation in the large domain. The initial velocity component at individual problem set is differently determined from a Maxwell-Boltzmann distribution and solutions from independent simulations are averaged to produce the final solution. The labour of manually administrating multiple job executions are resolved by using a BigJob framework, which is to be discussed in the Section 3.

Along with the advantage in computing capability, sampling multiple experiments provides another advantage of less-sensitivity to coupling conditions. Even if the coupling parameters are ill-chosen, highly noisy individual solution can be refined by the enough number of independent samples. This advantage also increases the value of capturing the magnitude of statistical noise in Section 2.4.1, because the requirement of predicting the macroscopic velocity in the sampled layer becomes less important.

2.5. Temporal Coupling Schemes

Two conventionally used coupling approaches of synchronized and sequential coupling strategies are depicted in Fig. 2. In synchronized coupling, CFD and MD codes exchange the information in the overlapping region at each sampling interval (denoted by Δt) and independently evolve to the next exchange timestep. In contrast, one domain advances to the next exchange timestep and leads its counterpart to approach this point in sequential coupling. Comparing these two mechanisms, synchronized coupling has a far better parallel efficiency because both codes independently evolve to the next sampling interval, while sequential approach is expected to produce more time-accurate solution because the boundary condition on following domain (CFD domain in the figure) is implicitly imposed. Unfortunately, both strategies contain the time-lagging phenomenon in CFD boundary region, because averaged molecular dynamic properties over backward sampling duration (from $n\Delta t - \Delta t_s$ to $n\Delta t$) represents the CFD boundary condition at that instance ($n\Delta t$). Extrapolation from previous MD solutions is necessary to eliminate the time-lagging by half of sampling duration ($\Delta t_S/2$) in the CFD boundary zone.
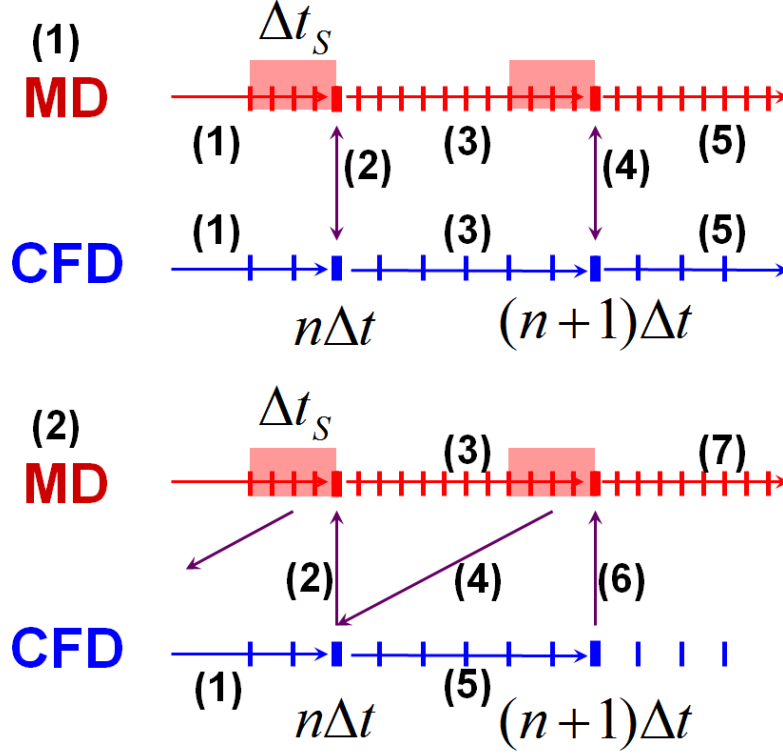
Figure 2: Conventional Time Evolution Mechanisms of a Hybrid CFD-MD Approach; CFD and MD codes are scheduled to conduct data exchange in the overlapping region at every Δt sampling interval. CFD solution at $n\Delta t$ is directly applied as the boundary condition for MD simulation and backward time-averaged molecular dynamic properties over Δt_S sampling durations are imposed as CFD boundary conditions. (1) Synchronized Coupling: Both codes communicate at the same time level and independently iterate to next exchange point. (2) Sequential Coupling: From the same time level, one solver advances to the next communication point and impose implicit boundary condition to its counterpart.

17

As is presented in Fig. 3-(0), Wang and He [10] proposed shifting the time axis of one domain by half of the sampling interval to eliminate this lagging effect. After both codes evolve by a sampling interval, the instantaneous CFD solution at $n\Delta t$ is communicated with averaged MD solution from $(n-1/2)\Delta t$ to $(n+1/2)\Delta t$. Two previous solutions from the counterpart are extrapolated to impose hybrid boundary conditions. The benefit of imposing extrapolated boundary condition is that the sampling duration can be designed as long as the sampling interval ($\Delta t_s = \Delta t$). However, the accuracy of extrapolated solution is worth to debate. In this scheduling, two *previous* CFD solutions at $(n-1)\Delta t$ and $n\Delta t$ are extrapolated to produce MD boundary conditions from $(n+1/2)\Delta t$ to $(n+3/2)\Delta t$. Except the velocity gradient is linear in time space, extrapolated properties fail to predict correct values throughout the simulation interval (from $(n+1/2)\Delta t$ to $(n+3/2)\Delta t$). The only way to reduce this extrapolation error is to reduce the sampling interval, which is contradictory to the condition for reducing the statistical error.

A new scheme named 'prediction-correction approach' is also depicted in Fig. 3. The main difference from the default model is that CFD code iterates additional time steps after the code evolved to the next data exchange time. For example, in Fig. 3-(1), CFD code additionally evolves by the half of sampling interval after the code approached to $n\Delta t$. CFD code sends these predicted properties at $(n+1/2)\Delta t$ to the MD site and receives averaged molecular properties around $n\Delta t$. CFD code loads its previous flow profile at $n\Delta t$ and runs the actual simulation to next communication point at $(n+1)\Delta t$. Clear benefit of current approach is that both solvers extrapolate their boundary conditions from *current* solutions (either exact solution or predicted values) instead of using *previous* history. This eliminates the sensitivity of extrapolated solution according to the size of sampling interval in previous model, which enables increasing the sampling interval.

This approach is further refined to increase the accuracy of the hybrid boundary condition by increasing prediction time scale. In Fig. 3-(2), the prediction time scale is increased by one more sampling interval. While MD solver evolves for one sampling interval, CFD code iterates to the next communication point of MD time space. This enables MD boundary condition being interpolated by predicted CFD profiles. Figure 3-(3) demonstrates the imposition of interpolated boundary conditions on both domains. In this formulation, CFD time space is shifted backward by one sampling interval and prediction step is scheduled to be $(5/2)\Delta t$.

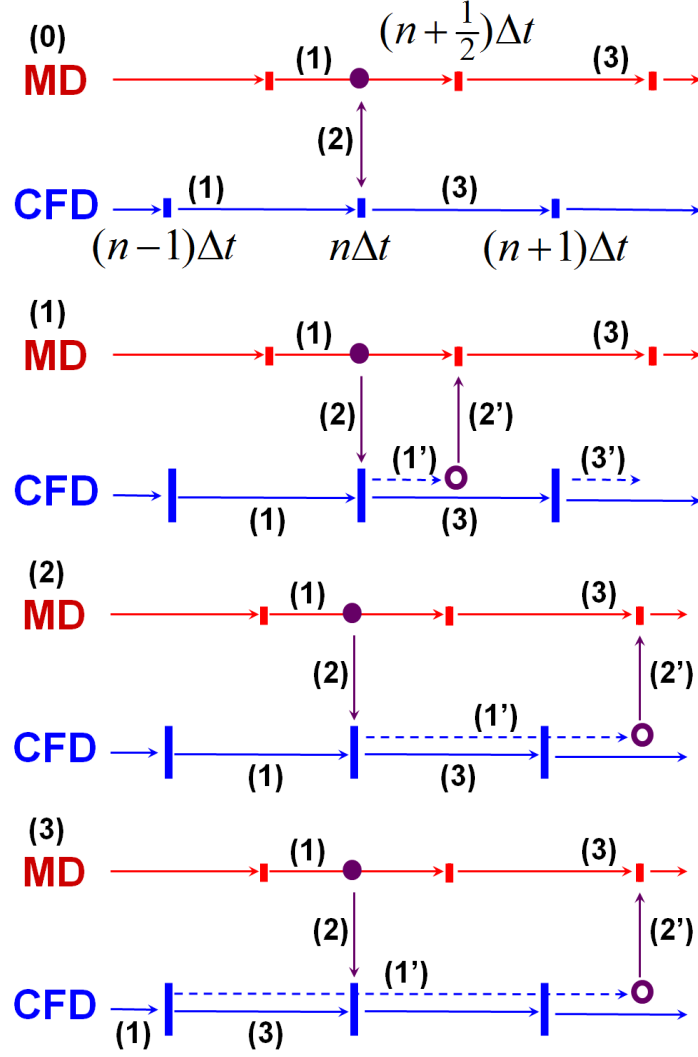Current numerical approach provides more accurate time-variant solution

Figure 3: A Prediction-Correction Approach with Extrapolated/Interpolated Hybrid Boundary Conditions; Applying extrapolation/interpolation enables increasing sampling duration as long as sampling interval. (0) Default Formulation; The hybrid BC in MD code is extrapolated from previous solutions. (1) Extrapolated Boundary; CFD code runs the prediction step by $0.5\Delta t$. MD code imposes the hybrid BC by the extrapolation from the current value. (2) Interpolated MD Boundary; CFD code runs the prediction step by $1.5\Delta t$. MD code imposes interpolated hybrid BC. (3) Interpolated Hybrid Boundary Conditions; Time axis of CFD domain shifts back by 1 sampling interval and the prediction step is set $2.5\Delta t$. CFD and MD domains impose interpolated hybrid BC.

19

by decreasing or eliminating the unfavorable overshoot/undershoot phenomena in extrapolations. Meanwhile, additional computational cost is inevitable for CFD simulation. We propose the current approach to be used in following conditions: (i) computational cost on CFD is quite smaller than that of MD, and (ii) the driving force which causes the flow variation is provided from the CFD domain. Without condition (i), additional computational overhead for prediction process will harm the simulation performance. If (ii) is not satisfied, the pattern of flow evolution cannot be predicted and the accuracy of the predicted solution is not guaranteed.

3. Coupled Concurrent Multi-Scale (Continuum-Molecular) Simulation Framework

Two important issues on the performance of hybrid simulations are co-scheduling and load-balancing. Both can be resolved by adopting a Pilot-job concept. We explain the design of a multi-physics simulation framework which operates in the form of a single Pilot-job and contains a load-balancing function between distinct tasks.

3.1. SAGA and SAGA-based Frameworks - An Efficient Runtime Environment for Coupled Multi-component Computations

The Simple API for Grid Applications (SAGA) is an API standardization effort within the Open Grid Forum (OGF) [31], an international standards development body concerned primarily with standards for distributed computing. SAGA provides a simple, POSIX-style API to the most common Grid functions at a sufficiently high-level of abstraction so as to be independent of the diverse and dynamic Grid environments. The SAGA specification defines interfaces for the most common Grid-programming functions grouped as a set of functional packages (Fig. 4). Some key packages are:

- File package - provides methods for accessing local and remote filesystems, browsing directories, moving, copying, and deleting files, setting access permissions, as well as zero-copy reading and writing

- Job package - provides methods for describing, submitting, monitoring, and controlling local and remote jobs. Many parts of this package were derived from the largely adopted DRMAA
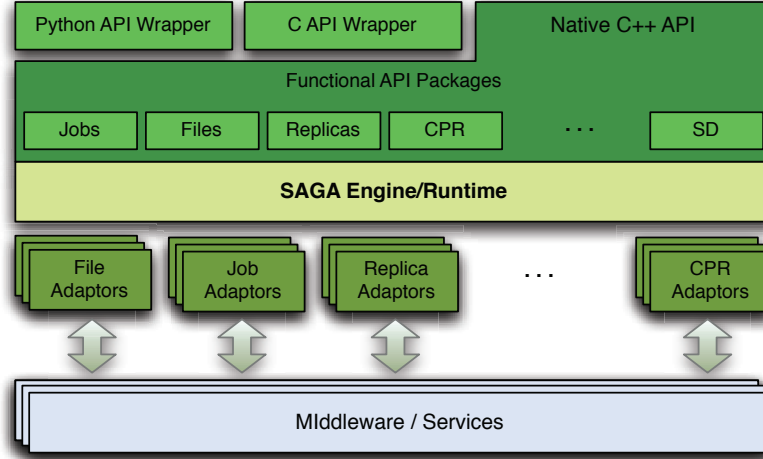
Figure 4: Layered schematic of the different components of the SAGA landscape. At the topmost level is the simple integrated API which provides the basic functionality for distributed computing. Our BigJob abstraction is built upon this SAGA layer using Python API wrapper

- Stream package - provides methods for authenticated local and remote socket connections with hooks to support authorization and encryption schemes.

- Other Packages, such as the RPC (remote procedure call) and Replica package

The BigJob [32] is a SAGA-based Pilot-Job, where a number of sub-tasks can run in a pre-defined schedule with the specified number of processors whether or not they are coupled. We basically devise this solution to overcome the concurrent scheduling requirement of coupled CFD and MD jobs and to dynamically allocate resources for load-balancing of these codes. The advantage of a BigJob over other Pilot-Job implementations is that this is infrastructure-neutral, thanks to various adaptors in SAGA.

Fig. 5 shows the structure of BigJob and its operation flow. When a BigJob is submitted to the remote resource, the application manager monitors the status of this Pilot-Job through the advert service. When resources are allocated to the BigJob, the application manager allots the obtained resources to its sub-jobs and a coupled simulation starts under the control of
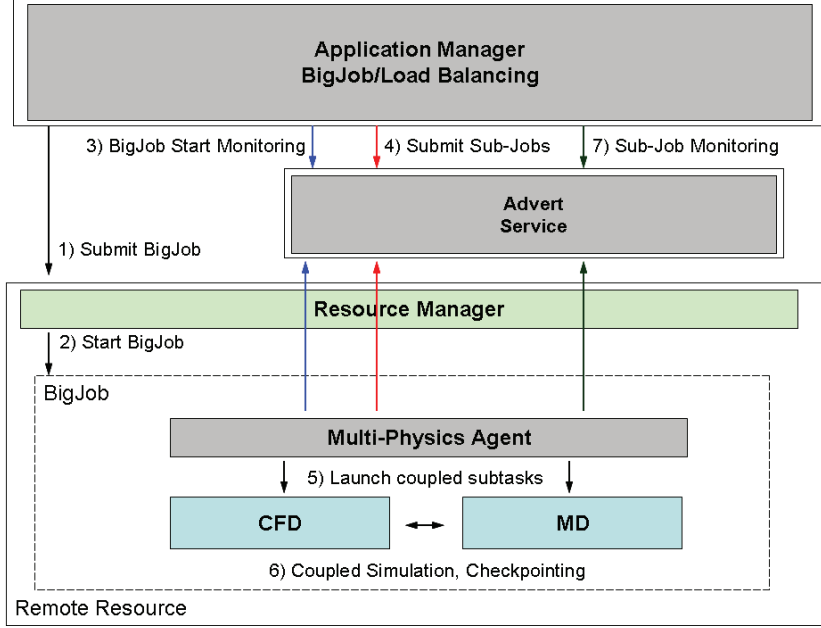
Figure 5: Architecture of the Controller/Manager and Control Flow: Application manager is responsible for job management including BigJob and sub-job submission, their status monitoring functions. We implement a load-balancing module, and migration service based on job information. Application agent system resides on each HPC resource and conducts job information gathering and also communicates with the application manager via the advert service

a multi-physics agent in the remote resource. Advert service keeps on getting the status of a Pilot-Job from the queuing system and the status of sub-jobs from multi-physics agent. It also delivers this information to the application manager by a push-pull mechanism. The application manager watches the status of sub-jobs and decides the next event when the coupled simulation is finished. If an individual simulation is of interest, the manager closes a BigJob allocation when the simulation is finished: In cases of multiple replica simulations or load-balanced coupled simulation, the manager relaunches sub-jobs on the same BigJob allocation until all replicas or load-balancing steps are completed.

3.2. Load-Balancing of Coupled Multi-Physics Simulation

Load balancing of a coupled simulation implies the flexibility to re-distribute resources to the individual task according to the performance of individual

22

job. We will discuss the implementation and algorithm of a simple load balancer (LB) [33]; it is important to mention that the LB functions in the context of the SAGA-BigJob framework.

The idea is to assign more resources to heavier sub-jobs under the fixed resource allocation, until all sub-jobs elapse the same execution time. As it is impossible to predict the performance of each code in advance, we let the LB monitor the wall-clock time between information exchange points of coupled tasks and iteratively change the processor distribution until the load balancing is achieved. As the individual solver is considered as black-box, each application code is assumed to have the ideal parallel efficiency: In case application codes are highly scalable, the LB can find the best condition after a few dynamic re-distributions. Also, all processors in one node are assigned to one single task to prevent the interference when multiple MPI tasks are running in a single node. ***Jeff: I found that the performances of MPI jobs decrease if more than two codes share a single node. For example, two 4-px jobs run at the same node of queenbee, performance of each code is half of one 4-px job: two codes share the same 4 processors and another 4 processors are idling. That's the same on Ranger. Looks as if the problem of default MVAPICH configuration, as I saw the same problem in KISTI.

Let the computation time (between exchanges) of the two sub-jobs be t_{CFD} and t_{MD}, and the number of processors assigned to each domain be PE_{CFD} and PE_{MD}, respectively. Subscripts C and N denotes current and next states. Assuming ideal parallel efficiency, total load of each application remains the same after resource re-allocation,

$$
\begin{aligned}
W_{CFD} &= PE_{CFD,C} \times t_{CFD,C} = PE_{CFD,N} \times t_{CFD,N} \\
W_{MD} &= PE_{MD,C} \times t_{MD,C} = PE_{MD,N} \times t_{MD,N}
\end{aligned}
\tag{11}
$$

In spite of the re-allocation, the total number of processors utilized remains the same:

$$
PE_{TOT} = PE_{CFD,C} + PE_{MD,C} = PE_{CFD,N} + PE_{MD,N}
\tag{12}
$$

Our objective is to reduce the computation time of a sub-job to the point until the two application components show the same computation between the exchange points, i.e., $t_{CFD,N} = t_{MD,N}$. From Eqn. 11 and Eqn. 12 an optimal number of processors distributed for the CFD subtask would be:

$$
PE_{CFD,F} = \frac{W_{CFD}}{(W_{CFD} + W_{MD})} \times PE_{TOT}
\tag{13}
$$

The MD simulation (sub-job) will follow a similar expression.

The above non-integer value proceed in discrete values expressed as the multiples of the number of CPU cores in a node. We choose the nearest discrete number to our load-balancing as the optimal number of processor on each application.

3.3. Implementation of an Execution Framework and Application-level Corrections

A hybrid CFD-MD framework is evaluated by implementing an application manager in Fig. 5, which is written in PYTHON script language. By default, an application manager calls a number of SAGA functions in sequence, to get allocated a vacant job, to run individual MPI simulation, to monitor its status, and to finalize the BigJob allocation.

In case the load-balancing capability is turned on, the situation becomes complicated. A single MPI job is not able to change its number of processors during the simulation. This implies that coupled codes should stop-and-restart to get assigned with changed number of processors. Thus, sub-jobs are scheduled to have multiple restarts from the previous checkpointing solution, which we denote 'load-balancing steps'. A LB is provided as a separate function in an application manager and is scheduled to run in between each restart of sub-jobs.

The efficient functioning of the LB is predicated on application codes being able to restart from their checkpointing data effectively. Application codes should also be equipped with generalized domain partitioning routine to run a simulation with any number of processors, without harming their parallel efficiency a lot. Another change implemented on application codes is the time checking routine. The runtime of each application is meaningless in running a LB since this runtime contains idle waiting on inter-domain information exchange as well as the individual computation time. This actual runtime can be counted by putting two wall-time functions before and after the information exchange routine.

The generation of an application manager and the changes in application codes raise the possible simulation scenarios as given in Fig. 6. The first (leftmost) shows the time evolution of a coupled simulation under a conventional job submission (which we define to be scenario S0), and others using a BigJob (denoted as S1). For S0, individual tasks with resource requirements of PE_{CFD} and PE_{MD} respectively, are independently submitted to the conventional queuing system and job scheduler recognizes these coupled tasks as

two distinct jobs. Thus, they start at different times on average. In this case, both tasks wait on the queue when no job is allocated (waiting stage), the first allocated job idles to perform data exchange with its counterpart (idling stage), and the actual simulation starts when both jobs are allocated (running stage). On the other hand, for scenario S1, a BigJob of size $PE_{CFD} + PE_{MD}$ is submitted to the queue, and coupled simulation directly starts when the resource is assigned to this BigJob. Because of co-scheduling of sub-jobs, a BigJob is free from long inactive mode which is frequent in conventional job submission, while total runtime is the same if the resource distribution to sub-jobs is identical. However, eliminating inactive mode in itself does not guarantee a reduction in the total runtime, because a larger single allocation may result in a greater queue waiting time than two simulations requesting smaller number of processors each (but the total being the same). The same situation can arise for the load-balanced case with one BigJob ($S1_{LB}$). From the comparison between S1 and S0, we can estimate the performance gain by concurrent start of distinct coupled codes; $S1_{LB}$ solution compared to other scenarios will demonstrate the benefit of a load-balancing function on coupled simulation.

4. Multi-physics Flow Simulations in Various Flow Conditions

A hybrid CFD-MD framework is employed to solve the multi-physics flow in nano-scale. Experimented problems are a sudden-start Couette flow and the oscillating boundary problem. We start from determining coupling parameters to the validation and verification of the hybrid simulation framework, then to the exploration of the moderate-speed flow simulation and time-accurate hybrid simulation.

4.1. Problem Description and Coupling Conditions

All applications we examine are internal flow fields filled with the liquid argon. Characteristic length of liquid argon is $\sigma = 3.405 \times 10^{-10}$ and time scale is $\tau = 2.2 \times 10^{-12}$. Density is $0.81m\sigma^{-3}$, which means 0.81 atoms are included in the characteristic volume. The fluid domain is a channel system which consists of two parallel plates placed in vertical direction. Liquid argon particles are filled in the domain and both walls have artificial properties which is the same as those of liquid argon. The slip ratio between fluid and solid particles are set 0.6, to satisfy the linear velocity gradient along the vertical direction. [7] Channel is 52 σ in height, which is O(10^{-8}) meters.
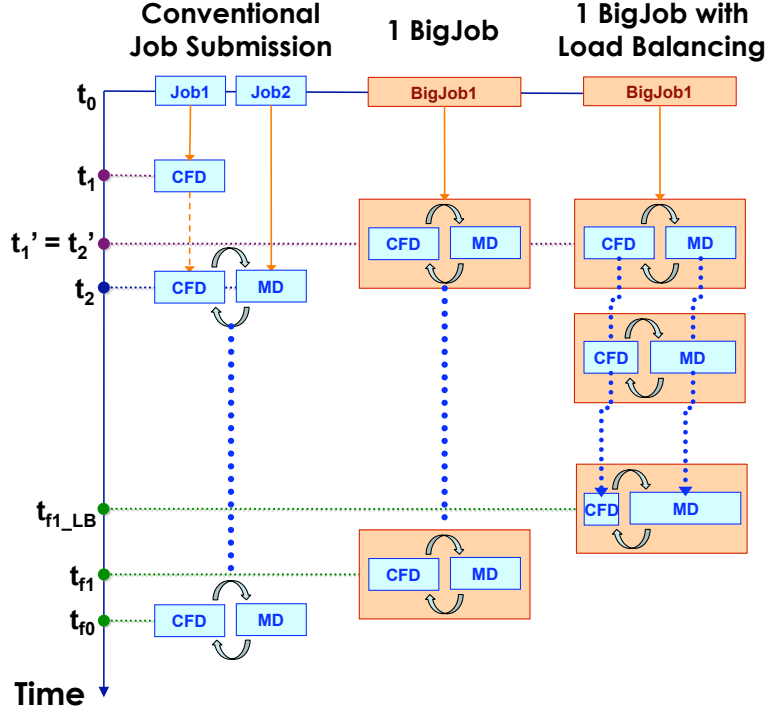
25

Figure 6: Comparison of dependencies encountered for coupled simulations submitted as conventional jobs, to the scenario when using Pilot-Jobs. Here we use only 1 BigJob (S1). The conventional mode of submission experiences three phases based upon their queue state: (i) All jobs are waiting: $(t_1 - t_0)$; (ii) Inactive mode (where one job is waiting for another: $t_2 - t_1$), and (iii) Active mode (running a coupled simulation: $t_f - t_2$). The Inactive stage, disappears when a coupled simulation runs within a BigJob, as an allocated BigJob distributes its resource to both sub-jobs.

Applications covered in this work are periodic systems in the perpendicular direction and the flow variation is derived by the horizontal motion of an upper plate.

As has been proposed in Sec. 2.4.1, we solve a stationary flow in particle domain to determine coupling conditions. Table 2 shows the averaged velocity depending on the layer size and sampling duration in 10^{-8} meter domain. Experiments were conducted with different lengths of the domain, changing from 35 σ to 70 and 140 σ. Noises around 0.2 height above the wall are presented.

From the individual test, we find that mathematical expressions on the strength of noise according to the height of sampled layer and sampling duration [15, 22] do not coincide with our experiment. From the first table, increasing the height of averaged layer from 0.1 to 6.4 σ reduces the statistical error by 4 times when sampling duration is 1 τ and this ratio even gets worse as sampling duration increases. The same situation also happens on sampling duration. This is contradictory to previous mathematical expressions which has been introduced in Sec. 2.4. From the data analysis, we figure out that the magnitude of sampling noise depending on the layer size and sampling duration is far more complicated: $V_N = a \times SD^b \times LH^c \times SD^{d \times ln(LH)}$, where V_N represents the velocity magnitude of the noise, SD denotes sampling duration and LH is the height of the layer. This equation is rewritten in simpler logarithmic formulation as,

$$ln(V_N) = ln(a) + b\ ln(SD) + c\ ln(LH) + d\ ln(SD)\ ln(LH)$$

and these coefficients in our specific case are as,

$$L = 35\sigma: \quad a = 33.67,\ b = -0.18,\ c = -0.30,\ d = 0.052$$
$$L = 70\sigma: \quad a = 25.85,\ b = -0.19,\ c = -0.27,\ d = 0.062$$
$$L = 140\sigma: \quad a = 17.78,\ b = -0.18,\ c = -0.25,\ d = 0.060$$

which directly expresses that 4 times longer sampling duration or 4 times larger layer height is far insufficient to half the noise.

Another result we observe from the above mathematical expression is that increasing the system size into the periodic direction is more effective in reducing the noise. Setting SD and LH to 1 τ and 1 σ, we find that the magnitude of the noise reduces from 33.67 to 17.78 if system size is quadrupled. This result supports previous mathematical expressions on statistical error.

27

Table 2: Statistical Error in Stationary Flow Simulation; Pure MD simulations of 35 × 52, 70 × 52 and 140 × 52 σ^2 are conducted. Liquid is bound in Y-direction by upper and lower walls and able to move in X-direction where periodic boundary condition is imposed. Initial data up to 100 τ are disregarded to provide enough time for minimization. Velocity of particles around the central layer are accumulated over 512 τ by using *fix-ave-spatial* function in LAMMPS package and post-processed to get the average velocity at different layer size and sampling duration conditions. Statistical noise becomes about half at 4 times bigger domain. The unit is 1/1000 of non-dimensional MD velocity (1σ / τ).

	$1\ \tau$	$2\ \tau$	$4\ \tau$	$8\ \tau$	$16\ \tau$	$32\ \tau$	$64\ \tau$
$0.1\ \sigma$	62.332	48.396	40.245	35.006	26.761	21.605	17.617
$0.2\ \sigma$	53.821	43.877	36.693	32.067	24.108	20.874	18.912
$0.4\ \sigma$	46.200	38.967	33.122	29.881	24.044	19.666	18.827
$0.8\ \sigma$	40.087	35.490	31.412	28.671	23.949	20.382	19.255
$1.6\ \sigma$	32.455	30.470	27.382	24.405	20.140	17.494	16.594
$3.2\ \sigma$	23.019	21.877	21.072	18.534	16.532	14.395	13.643
$6.4\ \sigma$	16.113	15.754	15.289	14.649	13.459	12.909	12.858
	$1\ \tau$	$2\ \tau$	$4\ \tau$	$8\ \tau$	$16\ \tau$	$32\ \tau$	$64\ \tau$
$0.1\ \sigma$	44.207	34.909	28.885	23.981	17.466	12.986	12.630
$0.2\ \sigma$	36.675	31.260	25.690	22.203	18.914	12.341	11.695
$0.4\ \sigma$	32.370	28.093	24.062	19.818	17.875	12.819	11.980
$0.8\ \sigma$	29.544	26.477	23.613	19.966	18.261	13.404	12.521
$1.6\ \sigma$	24.729	22.964	21.099	19.111	17.878	14.058	12.684
$3.2\ \sigma$	18.719	18.102	17.111	16.487	15.723	13.074	12.115
$6.4\ \sigma$	12.791	12.596	12.388	12.121	11.723	10.311	9.536
	$1\ \tau$	$2\ \tau$	$4\ \tau$	$8\ \tau$	$16\ \tau$	$32\ \tau$	$64\ \tau$
$0.1\ \sigma$	30.578	24.249	19.228	15.659	13.238	10.163	9.308
$0.2\ \sigma$	26.803	21.931	18.138	14.721	11.844	10.045	8.494
$0.4\ \sigma$	23.158	19.426	16.965	13.620	10.759	9.742	8.355
$0.8\ \sigma$	20.055	17.501	15.703	13.378	10.527	9.796	8.069
$1.6\ \sigma$	15.966	14.691	13.486	11.888	9.944	9.398	8.034
$3.2\ \sigma$	12.584	12.144	11.623	10.484	9.755	9.295	8.376
$6.4\ \sigma$	10.243	10.091	9.860	9.662	9.189	9.059	8.117

Following conclusions are deduced from the sampling noise analysis in the stationary flow. First, previous analyses on statistical error cannot be applied on wall-bounded nanoscale systems. As our empirical equation presents, the layer height and sampling duration are coupled together and noise reduction by handling these factors are less effective than have been reported. This emphasizes that the actual measurement of the sampling noise is inevitable to determine coupling parameters in the specific system. Second, increasing the size of sampling layer in the periodic direction is more effective on reducing the sampling noise. This leads us to an unfavorable conclusion that additional computational cost should be sacrificed to get the acceptable sampled solution.

Finally, CFD and MD computational domains are generated based on the above experiment, as depicted in Fig. 7. Pure MD region is specified to be 10σ, which was reported to be sufficient to prevent strong fluctuation between fluid particles and wall materials from directly transported to CFD domains. [11] This implies that the steady-state velocity in the hybrid domain will be around 0.2 σ/τ. We design the strength of the statistical error not to exceed 5 percent (≈ 0.01 σ/τ) of steady-state velocity. This lead us to set the width of MD domain in the principal flow direction as 140 σ, the cell size of CFD mesh to be 2σ in Y-direction, and sampling duration to be 10 τ. Two layer boundary zones from particle to continuum domain is placed ahead of pure MD region, from 10 to 14σ. Two layers of continuum to particle boundary is positioned from 18 to 22σ and external force region is place at the top of hybrid region, from 24 to 26σ.

4.2. A Sudden-start Couette Flow

A sudden-start Couette flow is simulated to verify the accuracy of the current framework with multiple sampling approach for the moderate-speed flow simulation. This application has been in wide use for the validation of a hybrid CFD-MD solver. [7, 11] The flow is initially set stationary and the upper wall starts moving by a constant velocity (1 σ/τ). This physical boundary condition of the continuum domain governs the evolution of the whole flow field. Figure 8 presents a sudden-start Couette flow profile by CFD, MD and hybrid simulations. Pure CFD produces identically the same result as analytic solution and MD simulations also describes the same flow physics though the slight fluctuation of the solution is observed. This verifies the accuracy of the individual solver. The hybrid solution also shows the slight deviation from the analytic solution, which is the fluctuation of
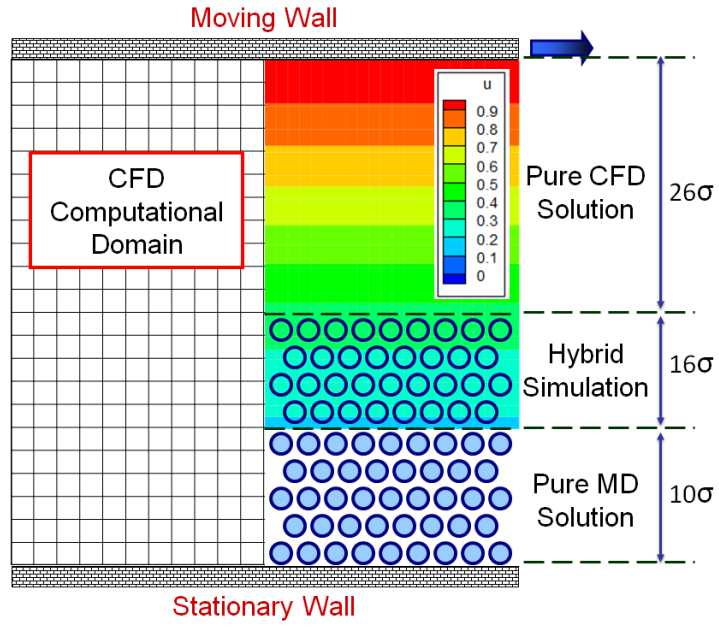
Figure 7: Computational Domain of Couette Flow Simulation; The height of the fluid domain is 52σ ($\approx 177\mathring{A}$). CFD mesh size is $71{\times}27$ and CFD cells at the pure MD region are treated as holes. MD domain size is about 140σ in the X-direction and around 26σ in the Y-direction, including the bottom wall. Periodic boundary condition is applied on the principal flow direction.

the sampled MD solution. Nevertheless, the hybrid simulation succeeds in demonstrating the same flow physics as the analytic solution. This variation can even be diminished if the solution is visualized over a longer temporal range, which is observed in many articles. This proves that the current hybrid framework accurately analyzes the steady flow profile in nano-scaled systems.

The flow condition in above experiment is rather unrealistic, which motivates us to apply the hybrid scheme to the analysis of moderate velocity flow. As has been expressed in Sec. 2.4.2, hybrid simulation of the low-speed flow field is mathematically possible but technically bound by the computing capacity, since the computational domain becomes u^2 times bigger in solving $1/u$ velocity field. We instead run u^2 independent simulations with the initial system size and different random number seeds in LAMMPS package.

The Couette flow profile with different numbers of samples are presented in Fig. 9. All configurations and parameters are identical to the above validation problem, except the upper plate velocity of 0.25 σ/τ. Changing the velocity to 1/4 implies that averaging 16 samples are required to get the acceptable numerical solution. The result supports the above supposition. The solution becomes very accurate when 16 individual runs are sampled. The reduction of statistical noise by multiple samplings is clearly verified by the graph in Fig. 10. The noise is roughly seen to reduce by half with 4 times more samples and the solution of sampling 16 runs shows about 5 % of the noise compared to the analytic solution profile.

The solution by multiple sampling is compared with the solution in increased system domain. Figure 11 shows the Couette flow profile with 16 times bigger system size in horizontal direction and the comparison of velocity variation in the middle of the overlapping region. From the result, both ways (multiple sampling and increasing system size) produce acceptable numerical solutions compared to the analytic solution. Interestingly, the scale of the noise compared to the analytic solution is very similar in both ways, which verifies that multiple sampling approach can replace the increase of system size to reduce the statistical error.

Collectively, results by multiple samples show the same order of accuracy compared to the increase of the system size. Especially in cases the physical system is large, multiple sampling is more effective than directly increasing the system size, because excessively large-scaled jobs (in view of wall-time limit or number of resources requested) are very hard to get allocated. In addition, the labor of manually submitting multiple independent runs and
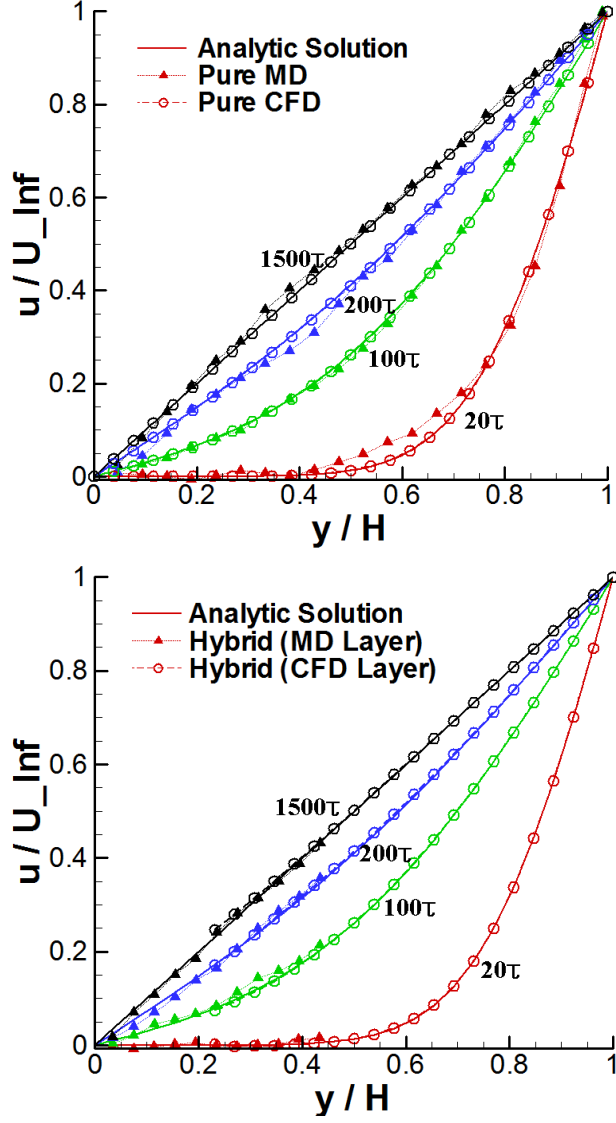
Figure 8: Unsteady Couette Flow Profile; The evolution of velocity field along the vertical direction is presented. CFD solution is the instantaneous profile at specified time and MD solution is spatially averaged over 2 σ in height and temporally averaged for 1 sampling durations ($=10\tau$). (Left) Pure CFD solution is exactly the same as analytic solution. MD solution shows the same flow pattern as analytic solution, though some fluctuation is observed. This verifies that CFD and MD represents the same flow physics. (Right) The steady result by hybrid approach produces the same numerical result as analytic solution, though the slight time-lagging in the hybrid boundary is observed during the evolution.

32
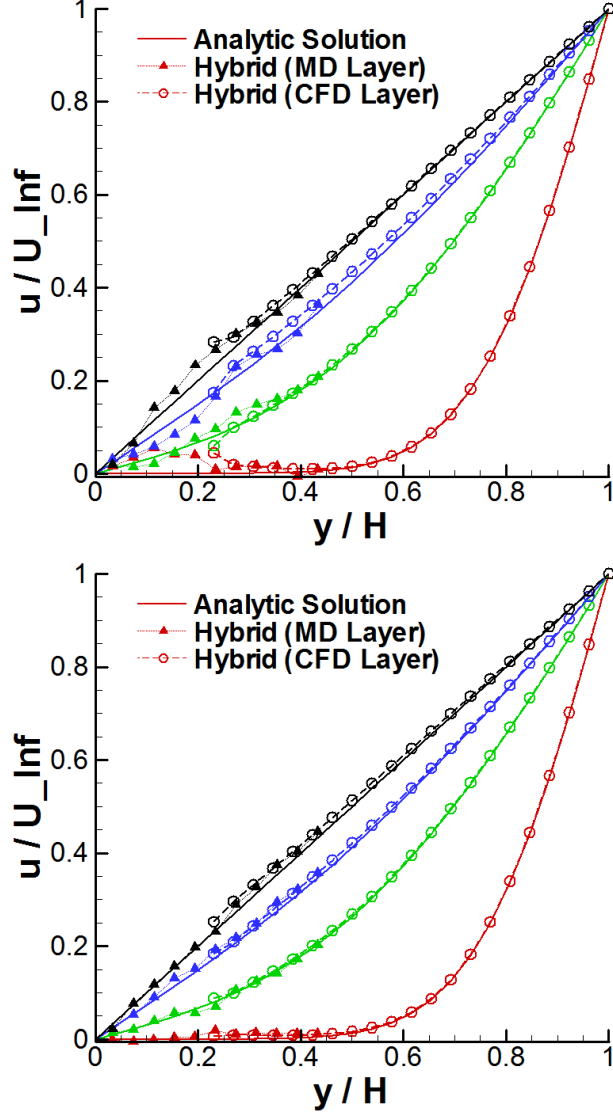
Figure 9: Couette Flow Profile with the Upper Plate Velocity of 0.25 σ/τ; The noisy solution when 4 individual simulations are averaged (left) is resolved by sampling 16 independent runs (right). Red lines denote the solution at 20 τ; Green, blue and black lines are solutions at 100, 200 and 1500 τ, respectively.
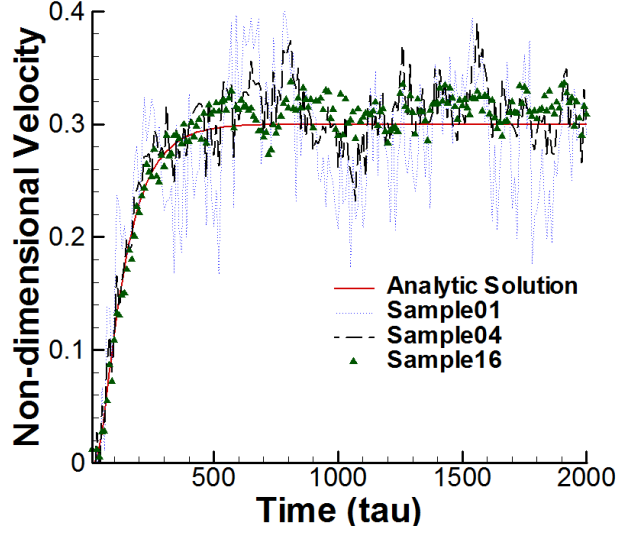
Figure 10: Variation of Continuum Velocity at the Position of 0.3 Height from the Bottom Wall (Middle of the Overlapping Region); Velocity changes at various sampling runs are compared with the analytic solution. In case 16 simulations are averaged, the noise is about 5 % compared to the analytic solution.

managing data sets can be relieved by adopting a BigJob framework.

4.3. A Physically Unsteady Flow Field: Oscillating Boundary Problem

The accuracy of designed temporal coupling scheme is verified by solving an unsteady oscillating boundary problem. In Couette flow simulation, which converges to a steady-state flow profile, the minor inaccuracy during the flow evolution can be eventually recovered. On the other hand, the inaccurate solution at an one instance harms the flow field afterwards in this physically unsteady problem. Therefore, the accuracy of temporal coupling scheme becomes more important. Also, velocity in the hybrid region becomes far slower than the Couette flow profile, so that the influence of noise from MD side is concerned to be more critical in the current flow simulation. The computational domain and coupling conditions are the same as the above Couette flow simulation. In this case, the upper wall boundary condition changes from the fixed velocity to oscillatory wall, which is $u_{wall}(t) = (\sigma/\tau) \times sin(2\pi t/T)$. Period T is set to be 200τ.

Figure 12 shows the oscillatory velocity profile by pure CFD and hybrid simulations. From the left figure, velocity profiles at each time instance are
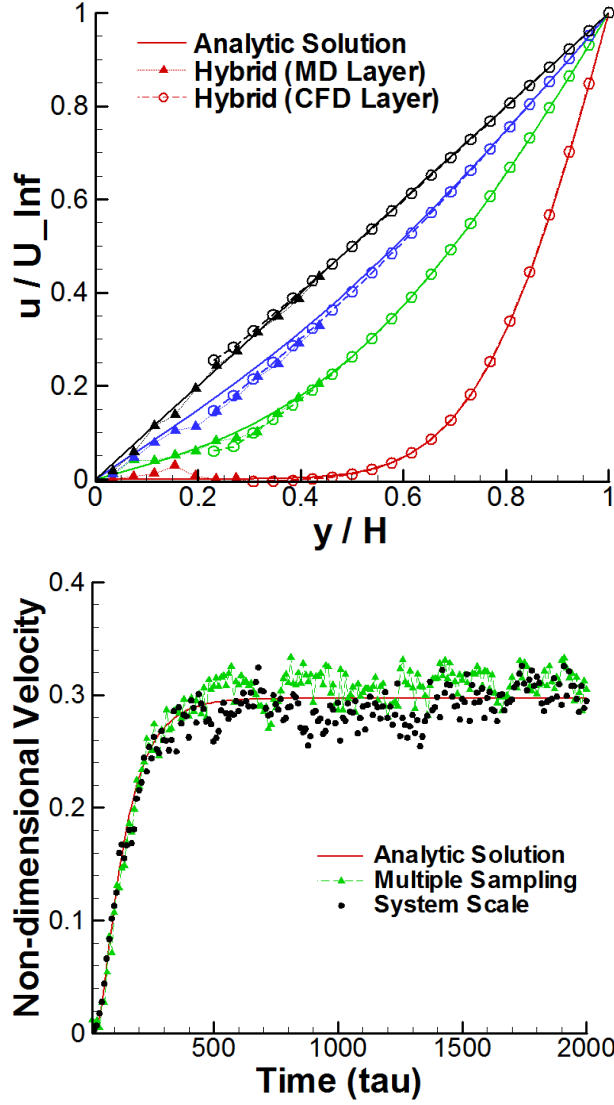
34

Figure 11: (Left) Couette Flow Profile in Increased System Size; Accurate flow profile can be obtained by increasing the system size 16 times larger when the velocity is reduced to 1/4. Red lines denote the solution at 20 τ; Green, blue and black lines are solutions at 100, 200 and 1500 τ, respectively. (Right) Variation of the Velocity in the Middle of Overlapping Region; Solutions by multiple sampling and increasing the system contain the similar strength of the noise in the solution, which is around 5 % of analytic velocity profile. This implies that multiple sampling approach can replace the increase of system size for solving moderate velocity flow.

35

roughly the same between the pure CFD and hybrid simulations in magnitude. This provides that the hybrid simulation approach is also applicable to time-varying flow simulations. Meanwhile, the temporal variation of the horizontal velocity in the middle of hybrid region expresses that the noise in hybrid solution is not negligible considering the ratio between continuum and hybrid velocities. We claim that this noisy solution is caused by the combination of sampling error and inaccurate temporal coupling scheme. To clearly examine the effect of temporal coupling scheme, we sampled multiple independent experiments and compared solutions by different temporal coupling schemes.

Comparing temporal evolutions of the velocity field by different coupling schemes in Fig. 13, the clear difference is the resolution of the overshoot/undershoot phenomena by the prediction-correction approach. Sufficient numbers of independent experiments are sampled to reduce the statistical error and prediction time scale of 2.5 sampling intervals is chosen on prediction-correction approach to impose the interpolated boundary conditions on both domains. On conventional model, the maximal error is seen at peak points. This is a natural characteristics of the linear extrapolation that it fails to predict the correct values around the strong variation. This inaccuracy is resolved by using a prediction-correction approach and applying interpolated boundary condition from predicted flow properties. However, another numerical inaccuracy of time-lagging pattern in conventional model is also seen in the prediction-correction model. This necessitates the implementation of higher-order interpolation schemes.

Plots in Fig. 14 quantifies the scale of inaccuracy according to the hybrid boundary condition imposition. In the conventional model, the velocity difference ranges from -0.017 to 0.015 σ/τ. The magnitude of this error reduces as we apply the prediction-correction approach and increase the prediction time scale from 0.5 (corrected extrapolation) to 1.5 (MD interpolation) and 2.5 (both interpolation) sampling intervals. The clear difference between the conventional extrapolation model and corrected extrapolation in prediction-correction approach demonstrates that the extrapolation from two "previous" properties contains a lot more error compared to extrapolating from the current value. The similar variation between extrapolation and MD interpolation in prediction-correction approach emphasizes that the accuracy of boundary condition in CFD domain is as important as the boundary condition in MD domain. Lastly, the solution error form the conventional model is reduced by half with the imposition of interpolated boundary conditions
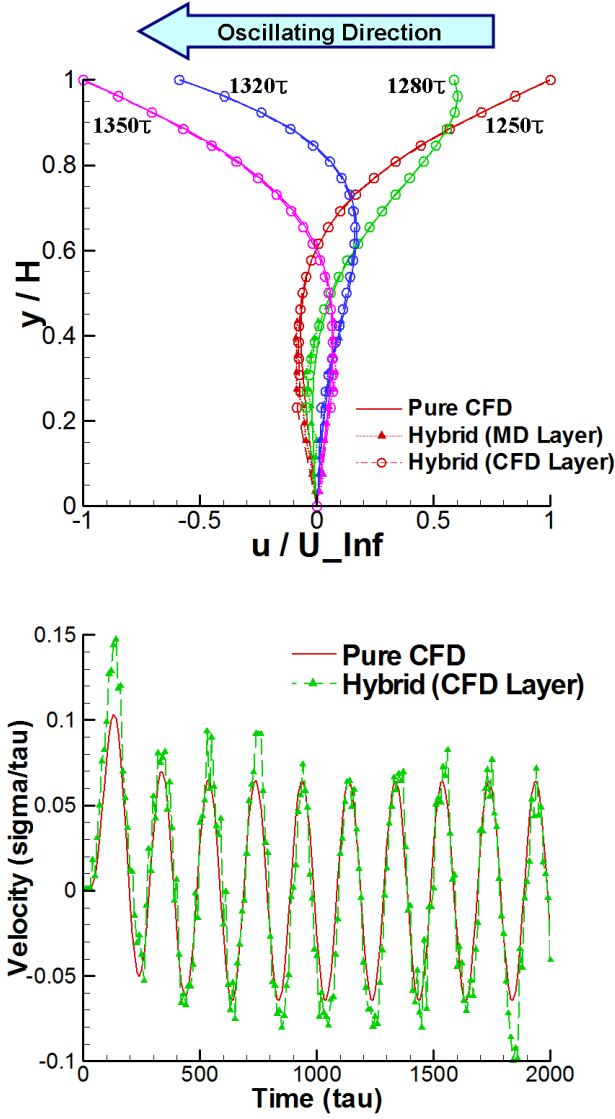
36

Figure 12: Unsteady Flow Profile of Stokes Boundary Layer Problem; (Left) Velocity profiles by pure CFD and hybrid simulations at specified time instances. Difference between hybrid and pure CFD solutions in hybrid region shrinks in the continuum domain. Noise from the MD simulation does not affect the global velocity profile a lot, because the driving force in this simulation is the oscillating velocity from CFD domain. (Right) Temporal variation of the velocity in the middle of hybrid layer. History of the velocity field reveals that the hybrid solution contains much noise in this experiment.
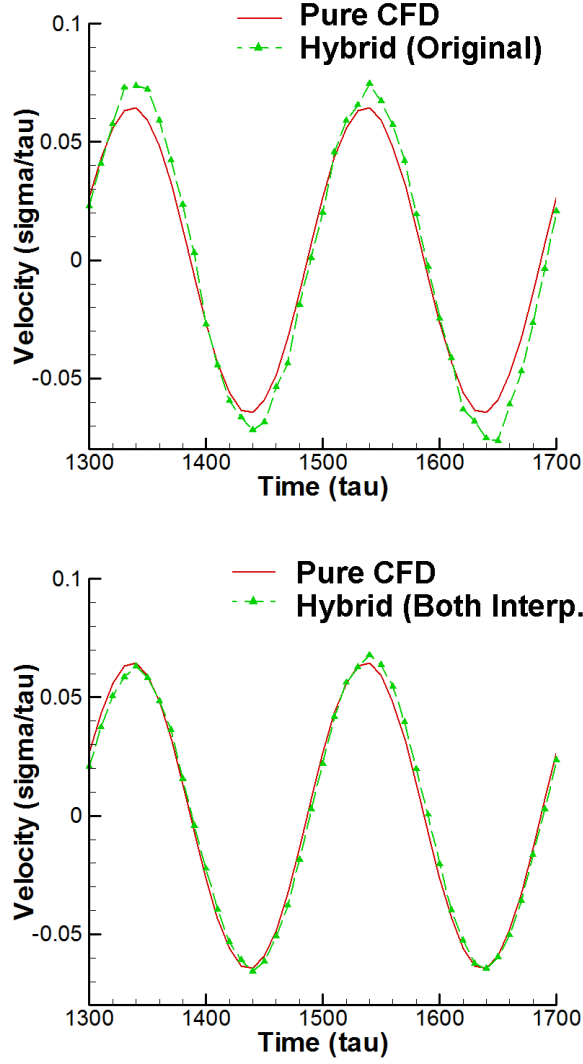
37

Figure 13: Temporal Variation of the Velocity in the Middle of Hybrid Layer; (Left) With conventional model, large overshoot/undershoot phenomena are observed on the peak points: the statistical noise around 0.01 σ/τ is nearly 20 % of continuum velocity. The time-lagging effect is also captured. (Right) Overshoot/undershoot phenomena in the conventional approach is almost resolved by applying the prediction-correction approach. The interpolated hybrid boundary conditions are imposed on CFD and MD domains.

Table 3: Effect of various configurations on waiting time. The tables show the queue waiting times on Ranger and QueenBee with a changing number of processors and different requested resource wall-time limits. Analyzing the actual waiting time as a function of the number of processors at different wall-time limits, it can be said that better more often than not, the waiting time decrease as the requested number of processors increases. The relationship between the waiting time and wall-time limit is harder to quantify. However, obtained numbers provide a good case study for showing the variance of actual queue waiting times.

Number of processors	Requested wall-time at 92±6% load (Ranger)				
	2hr	3hr	4hr	6hr	12hr
	Waiting time on the queue [sec]				
16	9989	15984	39151	65	66
32	15371	4106	11376	54	55
48	13264	4392	37780	43	44
64	9944	1975	39855	31	32

Number of processors	Requested wall-time at 95±4% load (Queenbee)				
	2hr	3hr	4hr	6hr	12hr
	Waiting time on the queue [sec]				
16	14339	3578	39113	6	940
32	14312	3550	39238	5	6344
48	21555	3517	39207	4	6353
64	21541	3489	39179	3	6329

on both domains.

5. Performance Analysis of a Multi-physics Simulation Framework

The benefit of a BigJob as a way of reducing the waiting time on the local queueing system can be discussed from our preliminary test of the relationship between the requested number of processors and the waiting time.

***Jeff: Already tested waiting time on Ranger: data table and expression will be replaced.

We designed experiments to determine if running larger and/or longer simulations effects the actual waiting time on the queue. We performed our experiments on machines spanning two orders of magnitude in size (and peak
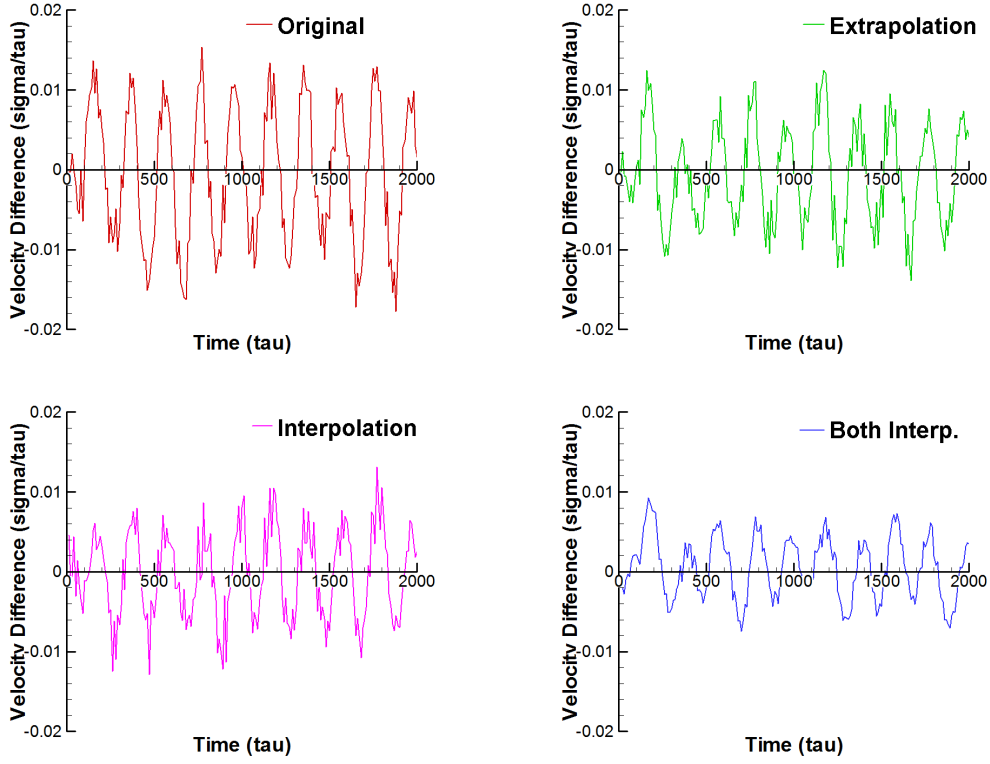
Figure 14: Reduction of Unsteady Error by Prediction-Correction Approach; Figures show the velocity difference between pure CFD and hybrid solutions in the middle of hybrid layer. Plotted data include the conventional extrapolation model and 3 different types of prediction-correction approaches, which are corrected extrapolation model, interpolated boundary model on MD domain and interpolated boundary condition on both domains. The velocity difference in the conventional model ranges from -0.017 to 0.015. This error reduces to be within -0.007 and 0.009 in refined model.

performance)– from approximately 500 px to 65000 px, and for a range of load-factors. We submitted jobs of different sizes, requiring different wall-time limits. Each time we submitted a job, we gathered the load-factor and the actual waiting time on the queue. Many factors effect the waiting times, arguably the most important of them are the load-factor at the instant of submission, requested wall-time limit and also the number of processors requested. Two other factors that effect this are the backfilling that occurs when some other unrelated job finishes and the changes in the priority of the test job when a particular higher priority job joins the queue; however, unlike the first three factors, the last two are somewhat random and it is difficult to systematically account for them. Also, the internal queueing policy of supercomputing centers may effect the waiting time on the queue based on their queueing priority including credential, fairshare, resource and service priority. As can be seen from Table 3, the waiting time tends to decrease as the number of processors requested in a job increases.

Results for machines with more than 5000 px, Ranger and Queenbee are presented in Table 3, and as can be seen, jobs with larger processor counts have typically lower wait times. The observation holds true for a range of values of requested wall-times over a range of "high" load-factors.

It is however, difficult to discern a relationship between waiting time with the requested wall-time limit of jobs; from experience there is greater variation in backfilling probability with varying wall-time requests. However, as we are able to establish that a single large job on average has to wait less at the queue than a smaller job does, most definitely the maximum wait time of two small jobs will be even greater. In other words the sum total of the waiting time (of the first-to-run job) and the inactive time (defined as the difference between the waiting time of the two jobs) will be larger than the wait time of a single large job.

***Jeff: Queue Wait Time Analysis: Waiting time of a BigJob and two conventional jobs. Emphasize the inactive time as well - it makes the conventional job submission to have longer wall time limit and it will even reduce the possibility of getting the backfilling capability. Include Table 2 here.

A BigJob submission shows the saving of waiting time on the queue, not only the bigger job size has the higher priority in the queueing system but also one BigJob submission eliminates the inactive idling time of first allocated job in conventional job submission.

***Jeff: More test conducted on Ranger. Table needs replacement.

Controlling runtime in these two scenarios, i.e., we take a BigJob of size

Table 4: Waiting and inactive time for conventional job submissions, and a single BigJob submission. All measured times are in seconds and expressed as 'mean±SD'. In both cases, conventional job is submitted to use 2×32 px and a BigJob requests 64 px on small and less crowded LONI clusters. Conventional job submission mode showed faster time-to-start (i.e., the sum of waiting time and inactive mode) on small problem size with 6 hr of wall-time limit, while a BigJob gets allocated faster with longer wall-time limit. Conventional job submission showed 3 failures during the test due to the timeover of wall-time limit in the first-started job.

| | Small simulation with 6 hr wall-time limit | | |
	Waiting time	Inactive mode	Failed runs
Conventional	12318±15649	7407±11375	2
1 BigJob	29452±31946	0	0

| | Large simulation with 24 hr wall-time limit | | |
	Waiting time	Inactive mode	Failed runs
Conventional	83102±77134	47488±55647	1
1 BigJob	76645±55474	0	0

2X and 2 conventional jobs of size X each, we compare the waiting time of a 64 px BigJob (with wall-clock limits of 2, 3, and 4hrs) which is smaller than the wait for a 32 px conventional job for the same values of wall-clock limits. As the individual simulations are assigned the same number of processors, the runtime performance will be similar in the two scenarios, and thus the total time-to-solution will determined by the wait-times on queues – which we show statistically to be lower for the larger BigJob submission mode.

Results for smaller systems (≈ 500 px) are presented in a different fashion in Table 4. In addition to the fact that a 64 px BigJob is now around 16% of the machine resources, the load-factors of the smaller machines fluctuated much more than those of the larger machines. Consequently the data obtained for smaller resources is far more noisier and than the "clean" data for the larger machines – Ranger and QueenBee. As can be seen from Table 4 although the waiting time for the first-to-start job was smaller in the conventional job submission mode than the BigJob (S1), the second job (convention job) had a large subsequent wait time; thus for conventional job submission mode there is a non-negligible inactive mode (defined as the time difference between queue wait times between the two simulations). There is no inactive

mode for BigJob submission as by defintion both simulations begin concurrently. Interestingly, the situation is somewhat worse for the conventional job submission; although the average wait time is lower than the BigJob, there exist 2 (out of 6) cases (for 6hr wall-clock limit), when the wait time of the second job is greater than the wall-clock limit for the first-to-start job. In other words, the second job fails to start in the duration that the first-to-start job is in active/run mode, but can't do anything useful as the second job is still waiting on the queue. This is typically alleviated with co-allocation of resources; however the number of production grid infrastucture that provide co-allocation (and co-scheduling) as a production service is very limited. This leads us to the heart of the advantage of the BigJob submission mode: circumventing the requirements of co-scheduling by providing an application level solution that preserves performance and guarantees non-failure due to large-fluctuations (see data for 24hr wall-time limit) in queue waiting times.

***Jeff: Runtime Analysis: Comparison of LB with conventional simulation time: different system size (with different ratio between CFD and MD), different number of simulation loop and different interval of simulation loop. Table 3 with 2 graphs - change of CPU allocation to each subjob with iteration time in 2 simulation cases. Mention the problem size and setting a little more detail.

Runtimes of the coupled simulation with a single BigJob is given on Table 5. For both small and large simulations, a default BigJob task takes about 1 percent longer than the conventional test. This is reasonable because a default BigJob has the same processor distribution between sub-jobs as the conventional job, while BigJob has the minor overhead of sub-jobs' status monitoring and communication with advert server. In cases of load-balanced BigJob simulations, there is a significant reduction in the runtime compared to successful conventional jobs – 13% and greater. For larger problem set, a load-balanced BigJob simulation relatively shows higher standard deviation (SD) due to the unexpected instability of a computing resource during one experiment, to be discussed in detail below.

The validity of a load-balancing function can be discussed by the change of processor distribution between subtasks throughout the simulation. For the result of a small simulation in Fig. 15, both CFD and MD subtasks are assigned with 32 px initially. After two simulation loops, a load balancer converges to the processor distribution of 12 to 52 px between CFD and MD respectively; this processor distribution remains the same until the simulation completes. Runtime per loop is reduced from 153 sec for the first loop to

43

Table 5: Results of runtime for S1, $S1_{LB}$ and conventional submission. All measured times are in seconds and expressed as 'mean±SD'. 6 distinct experiments were accomplished for each simulation, all with 64 px. In both cases, S1 shows about 1% overhead due to the communication with advert server. On the other hand, $S1_{LB}$ tests show about 13% runtime save compared to conventional submission.
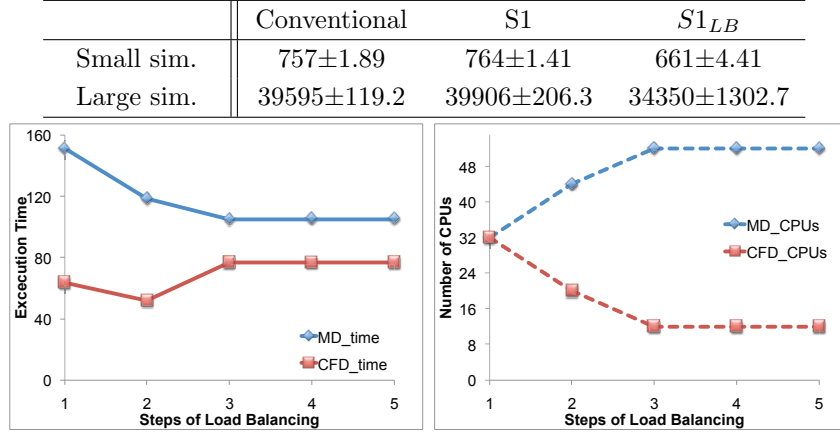
	Conventional	S1	$S1_{LB}$
Small sim.	757±1.89	764±1.41	661±4.41
Large sim.	39595±119.2	39906±206.3	34350±1302.7

Figure 15: Change of processor distribution between CFD and MD jobs and resultant computation time in the small simulation. A load balancer starts from the same number of processors assigned to both sub-jobs and detects 20 to 44 px between each sub-job as the optimal solution. The poor scalability of CFD job makes the load balancer to search for the optimal condition once again and the processor assignment finally reaches to a steady solution of 12 to 52 between two sub-jobs. Computation time for every simulation loop reduces from 153 sec to 107 sec after the balancing.

107 sec after the convergence. Total computation time is 596.19 sec, which is different from 663 sec counted from BigJob application manager. This time difference implies that the BigJob application manager spends about 13 sec per stage in executing its internal commands including the run of a load-balancing function and sub-job re-launch.

The result of computation time evolution for a large simulation is seen in Fig. 16. For most experiments, which is given in the left side of Fig. 16, a load balancer directly goes to a converged solution of processor distribution, which is 24 to 40 between CFD and MD jobs. On the other, in one experiment, computing nodes assigned to MD simulation seem to have temporarily

experienced the internal overhead as shown from the right side of Fig. 16. This overhead temporarily increased MD computation time a lot and a load balancer shows the fluctuating pattern of processor distribution in response to this temporary instability. A load balancer goes to a different steady solution after the system settled down, which is the processor distribution of 20 to 44 between two sub-jobs. Compared to the steady solution in stable cases, computation time for one simulation loop increases in this processor distribution increases from 1320 sec to 1380 sec.

Plots on the right side of Fig. 16 show a non-monotonically changing resource assignment by the LB, and thus demonstrating how the load balancer can be self-correcting and adapt to changing performance; after increasing the number of processors assigned to the MD, the load-balancer unassigns the additional processors.

6. Next Step: Further Refinement

The empirical mathematical equation on sampling noise has been presented in Sec. 4.1. We argue that this is a refined model compared to previous mathematical expressions. However, the formulation has not been verified by various systems and conditions: coefficients will be changing according to the distance from the wall, characteristics of fluid and solid elements, etc. More rigorous research is required to address a globally acceptable equation of sampling noise.

Unsteady flow simulation in Sec. 4.3 verifies that the prediction-correction approach provides more accurate solution than conventional temporal coupling scheme. The new approach is especially powerful in resolving the unfavorable overshoot/undershoot phenomena. On the other hand, the slight time-lagging effect in the conventional model has not been improved by the prediction-correction approach. We expect that this phenomenon can be resolved by applying higher-order extrapolation/interpolation on hybrid boundary regions.

7. Conclusions

Accurate and efficient multi-scale flow simulations by a hybrid CFD-MD simulation framework have been presented in this paper. Constrained Lagrangian dynamics equations of motion and file-based hybrid interfaces are implemented on a highly-reliable LAMMPS molecular dynamics package and
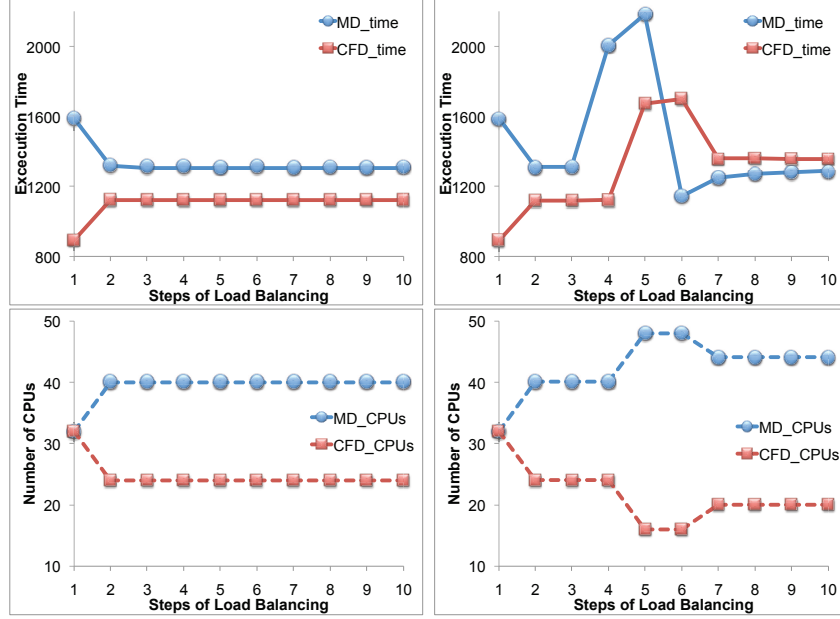
Figure 16: (Left Column) Change of processor distribution between CFD and MD jobs and resultant computation time in the large simulation. A load balancer directly finds the processor distribution of 24 to 40 between CFD and MD jobs and remains the steady state until it completes after 25 simulation loops. Initial computation time of 1605 sec reduces to 1320 sec after the convergence. (Right Column) Plots showing non-monotonic resource assignment by the LB, and thus demonstrating how the load balancer can be self-correcting and adapt to changing performance; after increasing the number of processors assigned to the MD, the load-balancer unassigns the additional processors.

a verified in-house incompressible CFD code. They are virtually integrated as a single BigJob framework.

A number of numerical issues which harm the accuracy of a hybrid solution have been explored. First, quantifying the sampling noise from a stationary flow has been proposed as a way of determining coupling parameters. We argue that our simple and intuitive idea unveils the influence of individual coupling parameter on the magnitude of statistical error and is very cost-effective in contrast to traditional trial-and-error approach. Moreover, the empirical equation derived from the stationary flow simulation describes that well-know mathematical expressions on statistical error are not accurate on nano-scale wall-bounded systems. Second, sampling multiple independent replicas has been introduced to refine the sampling noise of an individual solution and to explore to the low-speed flow regimes. This approach is superior to simulating a single large-scale problem set which is technically bound by computing capacity. The application to a Couette flow simulation in O(10) m/s velocity field is the first successful report of a moderate-speed flow simulation using a hybrid CFD-MD approach. Last, a prediction-correction approach has been designed for the accurate unsteady simulation. This approach acquires better solution by enabling the imposition of interpolated hybrid boundary conditions. The application to the oscillating boundary problem expresses that the current approach diminishes the overshoot/undershoot phenomena in the conventional methods.

Along with numerical issues, computational issues for the efficient coupled simulations have been also discussed. We introduced a BigJob framework and this directly solves the co-scheduling problem among logically separated sub-tasks. A simple load balancing function is also implemented on a BigJob framework, to achieve the load balancing among those separated-yet-coupled codes. From numerical experiments, we evaluate that a BigJob is very powerful in reducing the waiting time of the coupled simulation. Also, a simple load balancing function employed in a BigJob is effective in reducing the simulation runtime.

We emphasize that above numerical investigations ease the challenge to the hybrid simulation and broaden the application area. Also, our computational experiments contribute on how to efficiently conduct coupled simulations. ***Jeff: Plz fill this last paragraph!

Acknowledgements

References

[1] P. Koumoutsakos, Multiscale flow simulations using particles, Annu. Rev. Fluid Mech. 37 (2005) 457–487.

[2] A. Garcia, B. Alder, Generation of the chapman-enskog distribution, J. Comput. Phys. 140 (1998) 66–70.

[3] Q. Sun, I. Boyd, G. Candler, A hybrid continuum/particle approach for modeling subsonic, rarefied gas flows, J. Comput. Phys. 194 (2004) 256–277.

[4] D. A. Fedosov, I. V. Pivkin, G. E. Karniadakis, Velocity limit in dpd simulations of wall-bounded flows, J. Comput. Phys. 227 (2008) 2540–2559.

[5] D. A. Fedosov, G. E. Karniadakis, Triple-decker: Interfacing atomistic-mesoscopic-continuum flow regimes, J. Comput. Phys. 228 (2009) 1157–1171.

[6] S. T. O'Connell, P. A. Thompson, Molecular dynamics continuum hybrid computations: a tool for studying complex fuid flows, Phys. Rev. E 52 (1995) R5792–R5795.

[7] X. B. Nie, S. Y. Chen, W. N. E, M. O. Robbins, A continuum and molecular dynamics hybrid method for micro- and nano-fluid flow, J. Fluid Mech. 500 (2004) 55–64.

[8] X. Nie, S. Chen, M. O. Robbins, Hybrid continuum-atomistic simulation of singular corner flow, Phys. Fluids 16 (10) (2004) 3579–3591.

[9] J. Cui, G. W. He, D. Qi, A constrained particle dynamics for continuum-particle hybrid method in micro- and nano-fluidics, Acta. Mech. Sin. 22 (2006) 503–508.

[10] Y. C. Wang, G. He, A dynamic coupling model for hybrid atomistic-continuum computations, J. Comput. Phys. 62 (2007) 3574–3579.

[11] T. H. Yen, C. Y. Soong, P. Y. Tzeng, Hybrid molecular dynamics-continuum simulation for nano/mesoscale channel flow, Microfluid Nanofluid 3 (2007) 665–675.

[12] J. Liu, S. Chen, X. Nie, M. O. Robbins, A continuum-atomistic multi-timescale algorithm for micro/nano flows, Commun. Comp. Phys. 4 (5) (2008) 1279–1291.

[13] N. G. Hadjiconstantinou, A. T. Patera, Heterogeneous atomistic continuum representations for dense fluid systems, Comput. Phys. Commun. 4 (1997) 967–976.

[14] N. G. Hadjiconstantinou, Hybrid atomistic-continuum formulations and the moving contact-line problem, J. Comput. Phys. 154 (1999) 245–265.

[15] N. G. Hadjiconstantinou, A. L. Garcia, M. Z. Bazant, G. He, Statistical error in particle simulations of hydrodynamic phenomena, J. Comput. Phys. 187 (2003) 274–297.

[16] P. K. T. Werder, J. H. Walther, Hybrid atomistic-continuum method for the simulation of dense fluid flows, J. Comput. Phys. 205 (2005) 373–390.

[17] E. M. Kotsalis, J. H. Walter, E. Kaxiras, P. Koumoutsakos, Control algorithm for multiscale flow simulations of water, Phys. Rev. E. 79 (2009) 045701.

[18] E. G. Flekkϕy, G. Wagner, J. Feder, Hybrid model for combined particle and continuum dynamics, Europhys Lett. 52 (2000) 271–276.

[19] G. Wagner, E. G. Flekkϕy, J. Feder, T. Jossang, Coupling molecular dynamics and continuum dynamics, Comput. Phys. Commun. 147 (2002) 670–673.

49

[20] R. Delgado-Buscalioni, P. V. Coveney, Continuum-particle hybrid coupling for mass, momentum and energy transfers in unsteady flow, Phys. Rev. E 67 (046704) (2003) 1–13.

[21] R. Delgado-Buscalioni, P. V. Coveney, Usher: An algorithm for particle insertion in dense fluids, J. Chem. Phys. 119 (2) (2003) 978–987.

[22] R. Delgado-Buscalioni, P. V. Coveney, Hybrid molecular-continuum fluid dynamics, Phil. Trans. R. Soc. Lond. A 362 (2004) 1639–1654.

[23] G. Giupponi, G. D. Fabritiis, P. V. Covney, A hybrid method coupling fluctuating hydrodynamics and molecular dynamics for the simulation of macromolecules, J. Chem. Phys. 126 (2007) 154903–1–154903–8.

[24] S. E. Rosers, D. Kwak, An upwind differecing scheme for the time-accurate incompressible navier-stokes equations, AIAA J. 28 (1990) 253–262.

[25] S. Yoon, A. Jameson, Lower-upper symmetric-gauss-seidel method for the euler and navier-stokes equations, AIAA J. 26 (1988) 1025–1026.

[26] M. M. Rai, S. R. Chakaravarthy, An implicit form of the osher upwind scheme, AIAA J. 24 (1986) 735–743.

[27] B. V. Leer, Towards the ultimate conservative difference scheme. v. a second order sequel to godunov's methods, J. Comput. Phys. 32 (1979) 101–136.

[28] K. Travis, K. Gubbins, Poiseuille flow of lennard-jones fluids in narrow slit pores, J. Chem. Phys. 112 (2000) 1984–1994.

[29] [link].
URL http://lammps.sandia.gov

[30] J. L. Steger, F. C. Dougherty, J. A. Benek, A chimera grid scheme, Advances in Grid Generation FED Vol. 5 (1983) 59–69.

[31] Open Grid Forum. [link].
URL http://www.ogf.org/

[32] A. Luckow, S. Jha, J. Kim, A. Merzky, B. Schnor, Adaptive distributed replica-exchange simulations, Philosophical Transactions of the Royal Society A: Crossing Boundaries: Computational Science, E-Science and Global E-Infrastructure Proceedings of the UK e-Science All Hands Meeting 2008 367 (2009) 2595–2606.

[33] S.-H. Ko, C. Kim, O.-H. Rho, K. W. Cho, Load balancing for cfd applications in grid computing environment, KSAS International Journal 5 (2004) 77–87.